The Role of Cosmology in Shaping Physics Beyond the Standard Model

M.Sc. Thesis

By

Poonam Singh

Department of Physics
Indian Institute of Technology Indore
June 2022

The Role of Cosmology in Shaping Physics Beyond the Standard Model

A Thesis

Submitted in partial fulfillment of the requirements for the award of the degree

of

Master of Science

By

Poonam Singh

Department of Physics
Indian Institute of Technology Indore

June 2022

Indian Institute of Technology Indore

Candidate's Declaration

I hereby certify that the work which is being presented in the thesis entitled **The Role of Cosmology in Shaping Physics Beyond the Standard Model** in the partial fulfillment of the requirements for the award of the degree of **Master of Science** and submitted in the **Department of Physics, Indian Institute of Technology Indore**, is an authentic record of my own work carried out during the time period from July 2021 to June 2022 under the supervision of **Dr. Subhendu Rakshit, Professor, Indian Institute of Technology Indore.**

The matter presented in thesis has not been submitted by me for the award of any other degree of this or any institute.

Singh
31/05/2022

Signature of the student with date
(Poonam Singh)

This is to certify that the above statement made by the candidate is correct to the best of my knowledge.

Subhendu Rakshit 31.05.2022

Signature of the Supervisor of
M.Sc. thesis (with date)
(**Prof. Subhendu Rakshit**)

Poonam Singh has successfully given her M.Sc. Oral Examination held on **3rd June 2022**.

Subhendu Rakshit

Signature of supervisor of MSc thesis
Date: 05.06.2022

Convener, DPGC
Date: 07/06/2022

Signature of PSPC member no. 1
Date: 06/06/22

Signature of PSPC member no. 2
Date: 06/06/22

Acknowledgement

First and foremost, I want to thank my supervisor, Dr. Subhendu Rakshit, Professor, Department of Physics, Indian Institute of Technology Indore, for his remarkable guidance, unfaltering support, and relentless efforts. His zeal for science never ceases to astonish me. He is an amazing mentor with boundless patience and commitment. I can not thank him enough for all of his efforts on this project and beyond on so many levels.

Garvit Shrivastava deserves credit for keeping me calm and on track during the project's most challenging periods over the last year and a half.

I don't know how to convey my thanks and affection for my parents, who are the most important people in my life. They are the reason I am here, and they are the only individuals who have always been by my side in good times and bad.

Dedicated to my Mummy and Papa.

Abstract

The presence of dark matter (DM) and its characteristics are deduced indirectly from observed gravitational effects in astronomy and cosmology. The direct observation of weak gravitational lens effects near clusters, missing mass dilemma in the study of clusters and galaxies, the structure of galactic rotation curves, and the correspondence between the cosmic microwave background anisotropies and large-scale structure of the universe, could all be explained by the DM.

The Standard Model of particle physics (SMPP) is currently the best theory for characterizing all known fundamental particles. It is a quantum theory that uses quarks and leptons to describe the composition of all known matter. Except the gravity, SM can accommodate three of the four basic forces. The SM has significant limits, despite its success in understanding the cosmos. The SMPP does not contain any appropriate candidate for DM. As a result, new physics models are required to overcome the flaws of the SMPP. Any such physics might have an impact on the universe's early history.

This thesis is based on neutrinos and DM interaction. Our work is model independent. The amplitude and position of acoustic peaks in the cosmic microwave background (CMB) are altered as a result of these interactions, and a series of damped oscillations in the matter power spectrum are seen. By studying these impacts we can predict the features of dark matter particles. By reconciling the impact of dark matter and neutrino interaction on cosmological observations in comparison to the Standard Model of Cosmology, one can resolve one of the longest standing problems, the Hubble tension. Then, we obtain constraints on parameter space for such type of interaction using data obtained from Planck satellite and large-scale structure surveys. Thus, we can limit such proposed theories by applying cosmic limitations.

Contents

List of Figures

Chapter 1

Introduction

From Cosmological observation, we find that in our universe 85% of all matter is dark matter (DM) [1]. Dark matter is the composition of two words dark and matter, it is named “dark” because it does not interact with electromagnetic radiation (EMR) by reflecting, absorbing, or emitting it, so astronomers are still unable to observe it and therefore can only study its consequences on visible stuff and “matter” as it behaves like matter. Swiss astrophysicist Fritz Zwicky in 1933, studied the motion of the galaxies in the Coma cluster, during his research work at the California Institute of Technology, and summarized that DM exists [2]. Following that, measurements of whirling spiral galaxies, the implications of gravitational lensing on background objects demonstrated the presence of DM, and numerous pieces of evidence such as the Bullet cluster and the PLANCK satellite were recorded [3]. Furthermore, DM is an imperative ingredient in modelling and simulation of the early universe, the evolution of structures and galaxies, as well as having a detectable impact on CMB anisotropies. Notwithstanding its significance, we neither have concrete proof that DM exists nor the ability to comprehend its qualities.

The evolution of our universe is well described by the Standard Model of Cosmology (SMC), often known as the Hot Big Bang Model. The SMC, also known as the ΛCDM, is based on two key theoretical frameworks: the Standard Model of particle physics (SMPP), which covers physics at the quantum level, and the General Theory of Relativity (GTR), which covers physics at the classical level. It is based on the following assumptions: (1) the universe evolved from pure energy in the Big Bang, (2) the universe is made up of about 5% ordinary matter, 27% dark matter, and 68% percent dark energy, (3) the universe is isotropic and homogeneous on a cosmological scale, and (4) DM is assumed to be cold dark matter (CDM). However, there are issues when comparing SMC to SMPP, one of which is that no feasible candidate in particle physics (PP) satisfies all of the DM requirements. As a result, cosmology suggests that beyond the SMPP, new physics is required. This thesis aims to enlighten one part of the DM problem: DM interaction beyond gravity, i.e., DM-ν interaction. We wish to understand if such interactions are conceivable, what their impact would be, and how we may improve the accuracy of such models by applying cosmological constraints.

Before going into a detailed study of the DM-ν interaction, we go through the Big Bang's underlying principles in section [1.1] and its three major epochs that provide a piece of evidence for the presence of dark matter and predict its nature: Big Bang Nucleosynthesis (BBN) (in section [1.1.2]), Cosmic Microwave Background (CMB) (in section [1.1.3]), and Structure Formation (in section [1.1.3]). And we address various other pieces of evidence like the galactic rotational curve (in section [1.1.4]), and gravitational lensing (in section [1.1.5]) that predicts the existence of dark matter. Then we mention briefly all of the suggested alternatives for DM candidate in section [1.2]. We look for current DM status from collider search (in section [1.3.1]), direct search (in section [1.3.2]), and indirect search (in section [1.3.3]). The outline for the thesis is then given in section [1.4].

1.1 Expansion of Universe

According to Edwin Hubble in 1929, all galaxies are moving away from our galaxy at a rate which is proportional to their separation [4]. The Doppler shift of spectral lines may be used to calculate the speed [5]. The Big Bang model came into the picture as a result of this.

Let's look at how the universe has evolved with time, from the Big Bang to the present.

The universe will either grow or contract if it is thought to be isotropic and homogeneous. We consider two galaxies at $r(t)$ and $R(t)$ distances from our own. For isotropic and homogeneous expansion, the ratio

$$\chi = \frac{r(t)}{R(t)},$$

is constant in time [5]. As a result, when we differentiate in terms of time, we obtain

$$H = \frac{\dot{R}}{R} \tag{1.1}$$

here, H is called the Hubble parameter that measures how rapidly the cosmos expands at various distances from a given location in space and R is the scale factor that has value 1 for the present universe. The wavelength of light (λ_s) emitted by the source galaxy has been stretched out due to the expansion of the cosmos. So in terms of scale factor, the magnitude of the redshift (z) is expressed as,

$$1 + z = \frac{\lambda_0}{\lambda_s} = \frac{1}{R(t)}. \tag{1.2}$$

The wavelength of light that we detect is λ_0. If the recession speed (v) of the galaxy is substantially slower than the speed of light then, $z \approx v/c$. Because a photon's energy is inversely related to its wavelength, we may express temperature in terms of scale factor as

$$T(t) = T_0/R(t), \tag{1.3}$$

here T_0 is today's temperature of photons (found from CMB).

The Friedmann-Lemaitre-Robertson-Walker (FLRW) metric may be used to express four-dimensional space-time in an isotropic and homogeneous world as [6],

$$ds^2 = dt^2 - R^2 \left[\frac{dr^2}{1 - \kappa r^2} + r^2 \left(d\theta^2 + \sin^2 \theta d\phi^2 \right) \right]. \tag{1.4}$$

Here, ds^2 is the space-time interval, θ and ϕ are polar and azimuthal angles of the co-moving spherical coordinate system, and r is the co-moving radial distance.

If $\kappa = 0$, the universe would be flat, and if $\kappa \neq 0$, it would be curved. We will use the assumption that $\kappa = 0$ throughout this thesis. Since there are four components in the ΛCDM model that contribute to the energy density of the universe: DM, dark energy (expressed as cosmological constant Λ), baryons (ordinary matter), and radiation (photons and neutrinos). So total energy density is expressed as,

$$\rho(t) = \rho_{\mathrm{DM},0} R^{-3} + \rho_{b,0} R^{-3} + \rho_{\Lambda,0} + \rho_{r,0} R^{-4}. \tag{1.5}$$

Hubble parameter may be written in terms of the total energy density of the cosmos $\rho(t)$ using FLRW metric as

$$H^2(t) = \frac{8\pi G}{3} \rho(t), \tag{1.6}$$

here G is the Newtonian gravitational constant and equation (1.6) is known as the Freidmann equation [7].

Solving the Friedmann equation

To solve the above Friedmann equation, we need to know the dependency of ρ on time. For this, we derive the fluid equation from thermodynamics.

Fluid equation

The first law of thermodynamics for a system of energy U, temperature T, entropy S, and volume V, is,

$$dU = TdS - PdV. \tag{1.7}$$

Since no net heat flows across the boundary of volume because of symmetry. So,

$$dQ = TdS = 0. \tag{1.8}$$

On putting equation (1.8) in (1.7) and differentiating it with respect to time and then using $U = \frac{4}{3}\pi R^3\rho$ and $V = \frac{4}{3}\pi R^3$ we get,

$$3\frac{\dot{R}}{R}(\rho + P) + \dot{\rho} = 0 \tag{1.9}$$

which is the fluid equation. In this equation we have four unknown terms, so we will further simplify it using the Friedmann equation. On simplification, we get an acceleration equation which is discussed below.

Acceleration equation

On differentiating the Friedmann equation for the non-static case we get,

$$2\dot{R}\ddot{R} = \frac{8\pi G\dot{\rho}R^2}{3} + \frac{16\pi G\rho\dot{R}R}{3}. \tag{1.10}$$

Using equations (1.9) and (1.10) we get,

$$\frac{\ddot{R}}{R} = \frac{-4\pi G}{3}(\rho + 3P) \tag{1.11}$$

which is the acceleration equation. To solve this equation we need a relation between pressure and energy density. So, first of all, we will derive ρ and P and then relate them [5].

Number density, energy density, and pressure

To understand n, ρ, and P for various particles in the early universe, we need to know their distribution in phase space. For a homogeneous and isotropic distribution, phase space depends only on absolute value of momentum.
For relativistic particles, the distribution function is given by Bose-Einstein statistics for bosons ($-$) and Fermi-Dirac statistics for fermions ($+$). Both can be written as

$$f_{\pm}(p) = \frac{1}{\exp\left(\frac{E-\mu}{T}\right) \pm 1}.$$

At an early time, all particles were in thermal equilibrium with each other i.e., at the same temperature. The chemical potential[1] (μ) was small so can be neglected (used $\mu = 0$)[2].
If the internal degree of freedom is g, particle density[3] in phase space is given by

[1]The chemical potential of a species is the amount of energy that may be absorbed or released as a result of a change in particle number of the given species, $\mu = \delta G/\delta N|_T$.

[2]$\mu = 0$ means the number of particles and antiparticles are the same which is not true. So, a non-zero μ allows one to account for the baryon asymmetry. To make calculations easy, we are using $\mu = 0$.

[3]It is the density of the material that particles are composed of (gm cm^{-3}).

$g/(2\pi)^3 f(p)$. Here, $\pm$ sign is dropped to avoid cluttering.
To find number density[4] n, we integrate particle density over momentum as,

$$n = \frac{g}{(2\pi)^3} \int f(p) d^3 p$$

and,

$$\rho = \frac{g}{(2\pi)^3} \int E(p) f(p) d^3 p$$

also,

$$P = \frac{g}{(2\pi)^3} \int \frac{p^2}{3E(p)} f(p) d^3 p.$$

- **For relativistic case** $E(p) = \sqrt{p^2 + m^2} \approx p$ as $p >> m$. Then,

  For bosons

$$n_b = \frac{\xi(3)}{\pi^2} g T^3 \tag{1.12}$$

$$\rho_b = \frac{\pi^2}{30} g T^4. \tag{1.13}$$

  For fermions,

$$n_f = \frac{3}{4} \frac{\xi(3)}{\pi^2} g T^3. \tag{1.14}$$

$$\rho_f = \frac{7}{8} \frac{\pi^2}{30} g T^4. \tag{1.15}$$

  For a gas filled in container, change in momentum (velocity v) of particle due to collision with walls in x-direction is, $\delta p = 2p_x$. And total number of particles $N(p)$ with momentum space $= n(p) A \delta x$. So,

$$P = \frac{g}{3(2\pi)^3} \int d^3 p f(p) E(p) = \frac{1}{3} \rho. \tag{1.16}$$

- **For non-relativistic particles**

$$E(p) = \sqrt{p^2 + m^2} \approx m + \frac{p^2}{2m}.$$

  So,

$$n = g \left(\frac{mT}{2\pi} \right)^{\frac{3}{2}} \exp\left(-\frac{m}{T} \right), \tag{1.17}$$

[4] It is an intensive quantity that is used to describe the degree of concentration of countable objects in physical space (cm^{-3}).

also $\rho = mn$ and $P = nT$. Since $T << m$. So,

$$P \sim 0. \tag{1.18}$$

And pressure due to vacuum energy density is,

$$P = -\rho_\nu \tag{1.19}$$

So, using equations (1.16), (1.18) and (1.19), we can write a general form for pressure as,

$$P = \omega\rho. \tag{1.20}$$

Here, ω (variable) $= 1/3$ for relativistic particles, $\omega = 0$ for non-relativistic particles and $\omega = -1$ for vacuum energy. Using equations (1.13), (1.15) and (1.18) we get total energy density as [8],

$$\rho = \sum_i \frac{\pi^2}{30} g_i T^4 + \frac{7}{8}\sum_j \frac{\pi^2}{30} g_j T^4 = \sum \frac{\pi^2}{30} g_* T^4. \tag{1.21}$$

Here,

$$g_* = \sum_i g_i + \frac{7}{8}\sum_j g_j \tag{1.22}$$

and T is the temperature of the photon, which was measured from cosmic microwave background radiation (CMBR) as $T \approx 2.73$K. However because some particle types are no longer in thermal interaction with photons, they may have a different temperature. Neutrinos, for example, essentially separated from other particles before the annihilation of most positrons and electrons into photons. So, at present, neutrino temperature is roughly 1.95K.

As a result, we can write,

$$g_* = \sum_i g_i \left(\frac{T_i}{T}\right)^4 + \frac{7}{8}\sum_j g_j \left(\frac{T_j}{T}\right)^4. \tag{1.23}$$

Using equations (1.9) and (1.16) for the relativistic case we get,

$$3\frac{\dot{R}}{R}\left(\rho + \frac{\rho}{3}\right) + \dot{\rho} = 0.$$

On rearranging and integrating, we get

$$\rho \propto \frac{1}{R^4}. \tag{1.24}$$

Using equation (1.24) in equation (1.6) we get

$$\frac{\dot{R}^2}{R} \sim \frac{8\pi G}{3R^4} \sim \frac{1}{R^4}.$$

On solving we get, $R \sim t^{\frac{1}{2}}$. Hence,

$$H = \frac{\dot{R}}{R} = \frac{1}{2t}. \tag{1.25}$$

Using equations (1.9) and (1.18), for the non-relativistic case we get

$$3\frac{\dot{R}}{R}\rho + \dot{\rho} = 0.$$

On rearranging and integrating, we get

$$\rho \propto \frac{1}{R^3}. \tag{1.26}$$

For non-relativistic case, the Freidmann equation can be reduced as [8],

$$R \sim t^{\frac{2}{3}}.$$

So,

$$H = \frac{\dot{R}}{R} = \frac{2}{3t}. \tag{1.27}$$

Event	**Time**	**Temperature**
Planck epoch	$< 10^{-43}$ s	$> 10^{19}$ GeV
Grand unification	$< 10^{-36}$ s	$\approx 10^{16}$ GeV
Inflation	$< 10^{-32}$ s	$10^{15} - 10^{9}$ GeV
Electroweak symmetry breaking	≈ 150 s	$> 10^{19}$ GeV
Hadronization	$< 10^{-5}$ s	≈ 200 MeV
Neutrino decoupling	≈ 1 s	≈ 1 MeV
BBN	$10^{1} - 10^{3}$ s	$100 - 1$ keV
Recombination	≈ 370 kyr	≈ 0.4 eV
Present	≈ 13.8 Gyr	$\approx 10^{-2}$ eV

Table 1.1: Timeline of the expanding universe [9].

Table 1.1 shows the timeline of the expanding cosmos. Let us go over the three major epochs one by one.

1.1.1 Big Bang Nucleosynthesis epoch

During Big Bang Nucleosynthesis (BBN) epoch, neutrons and protons bind together to produce the primordial abundances of first light nuclei: H, He, tritium (^{3}H), ^{3}He, ^{6}Li, ^{7}Li, and ^{7}Be [5, 8, 10].

e^-, photons, ν_e, ν_τ, ν_μ, and their antiparticles are relativistic particles with temperature in the MeV range. So effective degrees of freedom (DoF) is, $g_* = 10.75$. Then from universe expansion we get,

$$tT^2 \approx 0.74 \text{ sMeV}^2. \tag{1.28}$$

Since protons are lighter than neutrons by $\Delta m \approx 1.3$ MeV, and till the reaction $\nu_e\, n \Leftrightarrow e^- p$ is favorable, the Boltzmann factor $\exp(-\Delta m/T)$, is found to suppress the neutron-to-proton ratio. The point where "freezes out" temperature reaches i.e., roughly at 0.7 MeV for neutron-to-proton ratio, above reaction slows down.

For non-relativistic particles, at freeze-out using number density, the neutron to proton ratio is given as,

$$\frac{n_n}{n_p} = \left(\frac{m_n}{m_p}\right)^{\frac{3}{2}} \exp\left(-\frac{(m_n - m_p)}{T}\right) \approx \exp\left(-\frac{\Delta m}{T}\right). \tag{1.29}$$

At $T_f \approx 0.7$ MeV (freeze-out temperature for neutron to proton ratio), $\frac{n_n}{n_p} \approx 0.16$. For T_f, the time is $t \approx 1.5$ seconds. Neutrons decay for around 3 minutes before being absorbed and forming deuterium and helium. As a result, from freeze-out through the commencement of deuterium production, the neutron to proton ratio will become,

$$\frac{n_n}{n_p} = \exp\left(-\frac{\Delta m}{T_f}\right) \exp\left(-\frac{t}{\tau_n}\right) \approx 0.13.$$

Here $\tau_n \approx 886$ sec, is the lifetime of the neutron.

Light nuclei synthesis after freeze-out

The synthesis of helium involves the following chain of reactions:

$$p\, n \longrightarrow d\, \gamma, \tag{1.30}$$

$$d\, p \longrightarrow {}^3\text{He}\, \gamma, \tag{1.31}$$

$$d^3\text{ He} \longrightarrow {}^4\text{He}\, p. \tag{1.32}$$

$E_{\text{bind}} = 2.2$ MeV is the binding energy of deuterium. At $t = 3$ min, deuterium production can be estimated by,

$$\frac{n_{\text{nuc}}}{n_\gamma} \approx \frac{n_{\text{nuc}}}{n_b} \approx 10^{-9}.$$

Over several minutes, all neutrons, except that decayed, produce helium abundance (Y_p) as,

$$Y_p = \frac{\text{mass of helium}}{\text{mass of all nuclei}} = \frac{m_{\text{He}} n_{\text{He}}}{m_N(n_n + n_p)} \approx 0.23.$$

Above we have used, $m_N \approx m_n \approx m_p \approx 0.94$ GeV, $m_{\mathrm{He}} \approx 4m_N$, and $n_{\mathrm{He}} = n_n/2$. The most accurate helium mass fraction was measured from 'metal-poor' galaxies as [11, 12],

$$Y_p = 0.238 \pm 0.002 \pm 0.005.$$

The first error is statistical, while the other is the result of systematic uncertainty.

Factors that may affect the abundance of helium

- Mean lifetime τ,
- Decoupling/ freeze-out temperature,
- Value of temperature relative to Δm.

Lithium Abundance

In the galactic halo, there are hot metal-poor stars that provide the most accurate estimates of lithium abundance. The lithium-to-hydrogen ratio [13], according to recent statistics, is

$$\frac{n_{\mathrm{Li}}}{n_{\mathrm{H}}} = 1.23 \times 10^{-10}.$$

The density of baryons measured by BBN is lower than the density of total matter. As a result, BBN provides strong evidence for DM not being baryonic.

1.1.2 Cosmic Microwave Background epoch

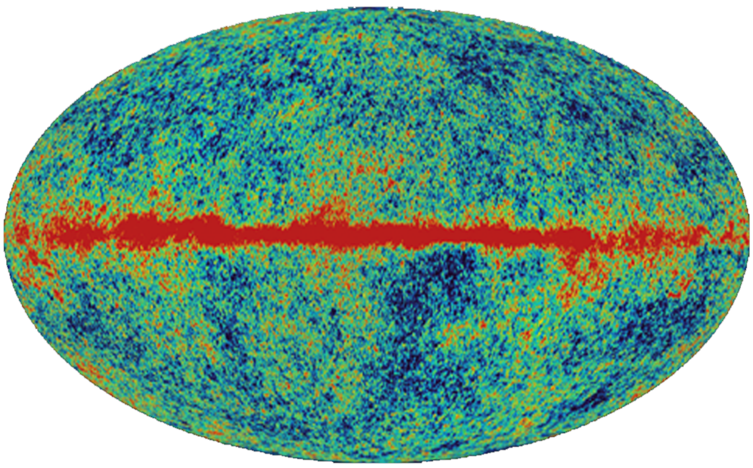

Figure 1.1: Cosmic Microwave Background map [14].

The cosmic microwave background radiation or CMB, is a thermal relic from a hot, dense period in the early cosmos that was discovered in 1965 by two American radio astronomers, Arno Penzias and Robert Wilson, at a wavelength of 73.5 mm and a black-body temperature of $T = 2.7255$ K [15, 16].

The Cosmic Background Explorer (COBE) satellite made the first reliable measurement over a broad range of wavelengths. The study of the COBE data yielded three significant results. First, at each angular position (θ, ϕ) on the sky, the spectrum of the CMB is remarkably close to that of a perfect black-body. Second, due to the net velocity of the COBE satellite relative to the isotropic frame of reference for the CMB, the CMB has a dipole distortion in temperature. Third, after subtracting the CMB's dipole distortion, the remaining temperature fluctuations have a tiny amplitude [17]. The successive space missions like COBE [17], Planck [3], and WMAP [18] have generated an increasingly precise map of CMB radiation across the whole sky.

CMB temperature measurement

The dimensionless temperature variation at a specific place in the sky is,

$$\frac{\delta T(\theta,\phi)}{T} = \frac{T(\theta,\phi) - \langle T\rangle}{\langle T\rangle} = \sum_{l=0}^{\infty}\sum_{m=-l}^{l} {a_l}^m {Y_l}^m(\theta,\phi).$$

Here, ${Y_l}^m(\theta,\phi)$ is the harmonic function. The root-mean-square temperature variation was calculated using the COBE Differential Microwave Radiometers (DMR) instrument [19] after subtracting the Doppler dipole as $\left\langle \left(\frac{\delta T}{T}\right)^2 \right\rangle^{\frac{1}{2}} = 1.1\times 10^{-5}$. The observations tells us that the CMB has a nearly perfect blackbody spectrum, so number density of black-body photons is given as

$$n_{\gamma,0} = \int_0^{\infty} n(\lambda)d\lambda = \int_0^{\infty} \frac{8\pi}{\lambda^4}\frac{1}{\exp\left(\frac{hc}{\lambda k_B T}\right) - 1}d\lambda = 4.11\times 10^8 \mathrm{m}^{-3}.$$

We can use this photon number density to find baryon to photon ratio (η) at present. For this we use Friedmann equation to get critical density as, $\rho_{cri} = 3H^2/8\pi G \approx 5200$ MeVm^{-3}. We use this critical density to find baryon density at present as, $\rho_{b,0} = \Omega_{b,0}\times\rho_{c,0} \approx 156$. Since, E_{baryon} (baryon energy) $\approx$ 939 MeV, so baryon number density is given as, $n_{b,0} = \varepsilon_{b,0}/E_{baryon} \approx 0.16$ m^{-3} and finally by taking ratio of this baryon number density with photon number density we get, $\eta = n_{b,0}/n_{\gamma,0} \approx 4\times 10^{-10}$.

The Statistical description of temperature fluctuations

During the measurement of CMB signal, the quantity measured at various points on the sky is the intensity at a certain frequency, which is given as I_ν. From the Planck's law for black-body we have,

$$I_\nu = \frac{2h\nu^3}{c^3\left(\exp\left(\frac{h\nu}{k_B T}\right) - 1\right)}.$$

For $h\nu << k_B T$, at a given frequency we get, $\delta I_\nu / I = \delta T / T$.

A statistical measure, the correlation function ($C(\theta)$) measures the temperature changes [16]. Take two locations on the decoupling surface or the surface of last scattering (SLS), r and r' with angular separation as $\cos\theta = \hat{r} \cdot \hat{r'}$. Then

$$C(\theta) = \left\langle \frac{\delta T(\theta_1, \phi_1)}{T} \frac{\delta T(\theta_2, \phi_2)}{T} \right\rangle_{r * r' = \cos\theta}, \tag{1.33}$$

$$C(\theta) = \sum_{l_1, m_1} \sum_{l_2, m_2} \left\langle a_{l_1 m_1} a^*_{l_2 m_2} \right\rangle Y_{l_1}{}^{m_1}(\theta_1, \phi_1) Y_{l_2}{}^{m_2 *}(\theta_2, \phi_2). \tag{1.34}$$

If the multipoles are random variables that are independent from one another, then the matrix of covariances $\left\langle a_{l_1 m_1} a^*_{l_2 m_2} \right\rangle$ is diagonal, i.e., $\left\langle a_{l_1 m_1} a^*_{l_2 m_2} \right\rangle \delta_{ll'} \delta_{mm'}$. Furthermore, if the temperature fluctuations are statistically isotropic, the multipole variances are independent of m, resulting in

$$\left\langle a_{l_1 m_1} a^*_{l_2 m_2} \right\rangle = C_l \delta_{ll'} \delta_{mm'}, \tag{1.35}$$

with

$$C_l = \frac{1}{2l+1} \sum_{m=-l}^{l} \left\langle | \, a_{lm} \, |^2 \right\rangle. \tag{1.36}$$

The set of C_l's forms the angular power spectrum. Using equation (1.35) in (1.34), and the addition theorem of spherical harmonics, we get

$$C(\theta) = \frac{1}{4\pi} \sum_l (2l+1) C_l P_l(\cos\theta). \tag{1.37}$$

Here, P_l is the Legendre polynomial. If temperature fluctuations follow a Gaussian distribution, the statistical distribution for each multipole has a zero mean ($\langle a_{lm} \rangle = 0$) and is completely described by only one parameter, the variance C_l. The temperature fluctuations are perfectly described by the two-point correlation function $C(\theta)$ in this situation. Consequently, the CMB spectrum is given as [20]

$$\Delta_T^2 = \frac{l(l+1)}{2\pi} C_l \langle T \rangle^2. \tag{1.38}$$

.

CMBfast [21], CAMB [22], and CLASS [23] are examples of effective and fast Boltzmann codes to compute the CMB spectrum for TT component, for a specific model of cosmology that are thought to be precise to at least 1% level.

The precise structure of the spectrum can thus provide vital details about the constituents of the universe and their interactions. Angular power spectrum from equation (1.38) is mapped in fig. 1.2.

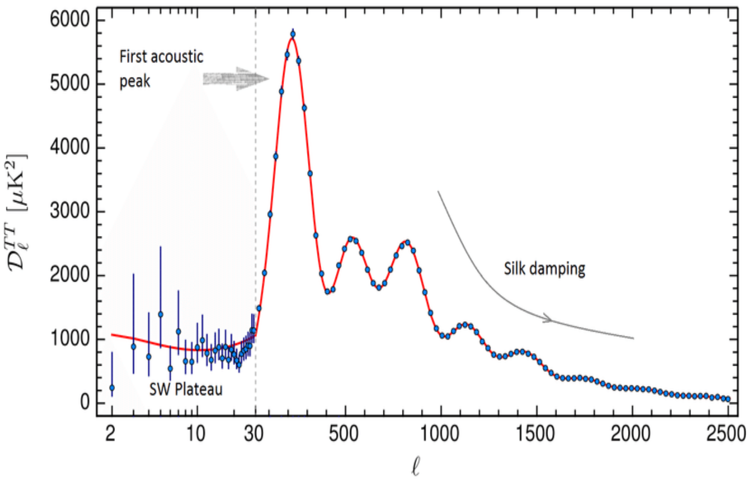

Figure 1.2: CMB spectrum for temperature anisotropies. This is the best-fit CMB spectrum obtained using the data of Planck Collaboration (2018) [3].

There are three possible regimes for the C_l. Let us discuss them one by one.

A regime with low l ($l \leq 100$)

When photons travel from the surface of last scattering to the Earth, it suffers from the gravitational potential fluctuations due to the large-scale structures. This effect is known as the integrated Sachs–Wolfe (ISW) effect. This effect gravitationally red-shifts CMB photons at large angular scales, causing tiny temperature fluctuations in the spectrum.

Regime for intermediate values of l ($100 \leq l \leq 1000$)

Consider the scenario just before the decoupling, where photons, electrons, and protons make a photon-baryon fluid. Dark matter has a threefold higher energy density than the baryonic matter. As a result, the photon-baryon fluid travels under the impact of gravitational force provided by the DM. The gravitational effect of dark matter will drive the photon-baryon fluid towards the core of the well if it falls into a dark matter potential well. As gravity compresses the photon-baryon fluid, the pressure rises. The fluid will eventually expand outward due to the increased pressure. The pressure reduces as the expansion proceeds, then gravity makes the fluid to collapse again. This to and fro cycle that has been established continues until photon decoupling occurs. These rarefied and compressed oscillations of the photon-baryon fluid are defined as acoustic oscillations. As a result, modes trapped at the extremes of their oscillations generate acoustic or Doppler peaks in the CMB power spectrum. These peaks can be seen in fig. 1.2. Let us discuss the information given by these peaks.

- **First Doppler Peak position**

  The number of oscillations completed before recombination corresponds to the different modes. The biggest peak for temperature anisotropies is subtended by the longest wavelength mode [24]. To find the position of the biggest peak of CMB spectrum we use FLRW metric.

  From FLRW we have

$$dt = \frac{Rdr}{c(1-\kappa r^2)^{\frac{1}{2}}}. \tag{1.39}$$

  From perfect fluid approximation, we have effective energy density as,

$$\rho = \rho_m + \frac{\Lambda c^4}{8\pi G}. \tag{1.40}$$

  Using equation (1.40), and the Friedmann equation we get,

$$H^2 = \frac{8\pi G\rho_m}{3c^2} - \frac{\kappa c^2}{R^2} + \frac{\Lambda c^2}{3}. \tag{1.41}$$

$$\Omega_{m,0} = \frac{8\pi G\rho_m}{3c^2 {H_0}^2} \tag{1.42}$$

$$\Omega_{\kappa,0} = -\frac{\kappa c^2}{R^2 {H_0}^2} \tag{1.43}$$

$$\Omega_{\Lambda,0} = \frac{\Lambda c^2}{3{H_0}^2}. \tag{1.44}$$

  Using equations from (1.41) to (1.44), $\rho_r \propto 1/R^4$, relation between R and z along with the condition $\Omega_r + \Omega_m + \Omega_\Lambda + \Omega_\kappa = 1$ where $\Omega_\kappa = 0$ for flat universe, we get,

$$dt = {H_0}^{-1}(1+z)^{-1}\left[(1+z)^2(1+\Omega_{m,0}z) + z(z+2)\left[(1+z)^2\Omega_{r,0} - \Omega_{\Lambda,0}\right]\right]^{-\frac{1}{2}} dz. \tag{1.45}$$

  For a flat universe, the distance of the last scattering depends on Ω_m and Ω_Λ, which can be find out as

$$\text{(comoving) } r_{\text{SLS}} = \frac{c}{H_0}\int_0^{z_l} \left[\Omega_m(1+z)^3 + \Omega_\Lambda\right]^{-\frac{1}{2}} dz.$$

  Here, r_{SLS} is the distance travelled by light between surface of last scattering (SLS) and us. From the perfect fluid approximation we have speed of sound (c_s) as

$$c_s = \frac{c}{\sqrt{3}}. \tag{1.46}$$

Using binomial expansion, we can expand the integrand term in the above integral to make integration simple. Since angular diameter distance (d_{SLS}) at SLS is given as,

$$\text{(proper) } d_{\mathrm{SLS}} = \frac{r_{\mathrm{SLS}}}{1+z}.$$

So,

$$\theta_{\mathrm{SLS}} \approx \frac{d_{\mathrm{SLS}}}{r_s} \approx 0.74\sqrt{1+z_s}(9 - 2\Omega_m{}^3) \approx 221. \tag{1.47}$$

The location of the first peak is consistent with the flat universe assumption [25].

- **Second peak**

  When the gravitational influence of the baryons is taken into account, oscillations become asymmetric as the fluid feels more gravitational force towards the core of the potential well than the outward expanding pressure. The impact on the power spectrum is to enhance the compression peak amplitudes compared to the rarefaction peak amplitudes. Another effect of baryon loading is that all peaks move to somewhat higher multipoles l.

  By looking at the impact of baryons on the location and amplitude of acoustic peaks in the temperature (TT) component of CMB spectrum, density of the baryons may be determined.

- **Third peak**

  The third peak measures density of the dark matter.

A regime with high l ($1000 \leq l$)

The acoustic peaks are attenuated at small angular scales because of silk damping [26]. This is the mechanism by which photons spread from over-dense to under-dense places during recombination, pulling baryons behind them and making the cosmos more isotropic. The damping tail validates the consistency of the underlying assumptions.

The concept that CMB photons are linearly polarised via Thomson scattering with electrons, whether during re-ionization or thermal decoupling , is a key feature. CMB polarization observations are essential because they give a second approach for extracting cosmic parameters and may be used to independently evaluate the predictions of several theories other than the CDM.

Polarization

We often describe the linear polarization with the help of two Stokes parameters [27] as, $Q = \langle E_x^2 \rangle - \langle E_y^2 \rangle$ and $U = \langle E_a^2 \rangle - \langle E_b^2 \rangle$. The electric field amplitude is E, the expectation value is denoted by angular brackets, and the subscripts show the standard Cartesian basis (x, y) and a 45^0 rotated Cartesian basis. Geometrically, separating the polarization pattern into two parts one with a divergence (the E-mode) and another with a curl (the B-mode), is more comprehensible. These modes are connected geometrically with the parameter U through a non-local transformation and they are independent from the coordinate system.

In the case of an under-density and an over-density, the patterns of E-modes and B-modes are shown in Fig. 1.3.

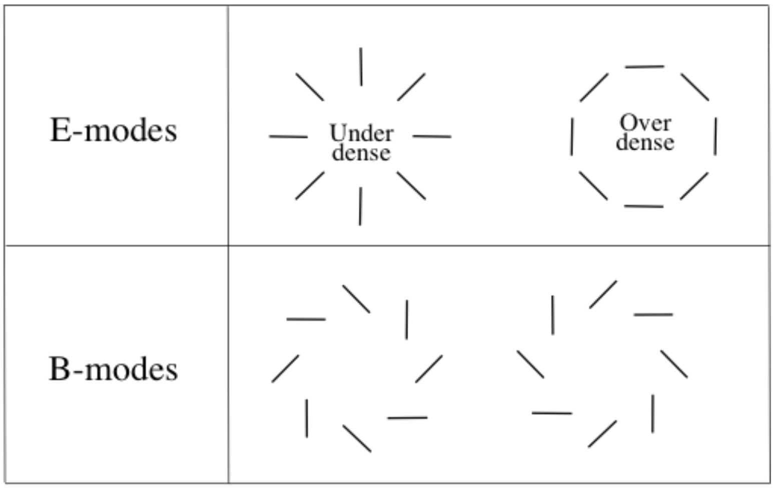

Figure 1.3: E and B modes, CMB components with no curl and no divergence [28].

There are six cross powers in theory which can be obtained from:

$$C_l^{i,j} = \frac{1}{2l+1} \sum_{m=-l}^{l} a_{lm}^i a_{lm}^{j*}. \tag{1.48}$$

where $i, j \in T, E, B$, will contain all of the temperature and polarisation details. However, the E modes pattern possesses mirror symmetry (as it is a scalar field), whereas pattern of the B modes is anti-symmetric (as it is a pseudo-scalar field), as seen in Fig. 1.3. This shows that $C_l^{TB} = C_l^{EB} = 0$, leaving four observables: $C_l^{TT}, C_l^{EE}, C_l^{BB}$ and C_l^{TE}. Only density fluctuation produces E-mode polarization pattern for CMB photons, but primordial gravitational waves caused by inflation, produces both E and B modes [29].

1.1.3 Structure formation

The matter power spectrum (MPS), $P(k)$ is used to describe the distribution of matter in the universe as

$$\left\langle \delta(k)\delta(k') \right\rangle = (2\pi)^3 P(k) \delta^3(k - k'), \tag{1.49}$$

here $k = 2\pi/\lambda$ is the wave-number, λ denotes the spatial scale, $\delta(k)$ represents the Fourier transformation for the density inhomogeneity $\delta(x) = [(n(x) - \bar{n})/\bar{n}]$, average over the whole distribution is shown by the angular brackets, and the Dirac delta function is denoted by $\delta^3(k - k')$. The variation in the matter density distribution is expressed by the $P(k)$, it will be large only if under-dense and over-dense areas are in large number, and small if there is a smoothness in density distribution. MPS from the equation (1.49) is mapped as:

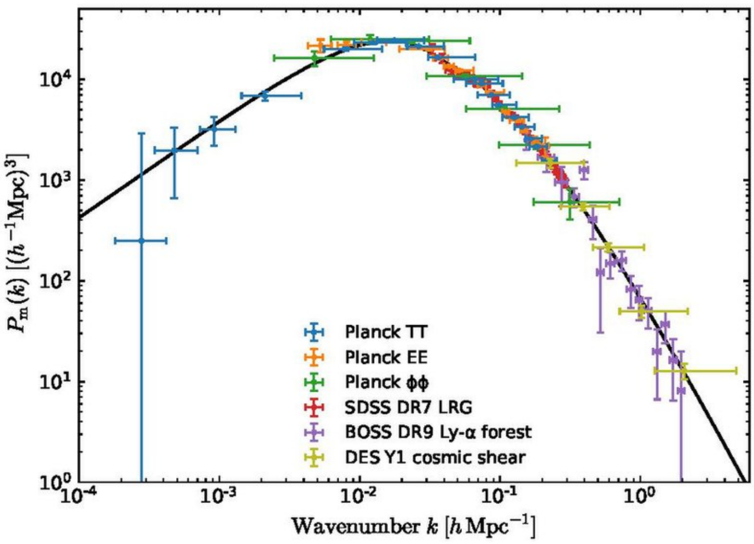

Figure 1.4: Matter Power Spectrum with massless neutrinos. This is the best-fit matter power spectrum obtained from Planck Collaboration (2018) [3].

Structure generation is based on the premise that minor density fluctuations are enhanced by the gravitational pull to form large-scale structures (LSS). In the early cosmos, there is no commonly chosen length scale due to inflation, so the primordial MPS goes along with a simple power-law as $P(k) = Ak^n$, here spectral index (a number) is denoted by n and A denotes the amplitude. From the Planck data for ΛCDM we get n or $n_s = 0.968 \pm 0.006$ and A or $A_s = (2.14 \pm 0.06) \times 10^{-9}$m [3]. In the strongly linked photon-baryon fluid, the conflicting forces of radiation pressure and gravitational pull generate baryon acoustic oscillations (BAO). Gravitational pull and photon pressure operate as the restoring and driving forces respectively on the baryons, which start behaving like a driven harmonic oscillator. The electrons responsible for scattering photons got confined in neutral hydrogen during the recombination phase. Photons diffuse out of over-dense places as their mean free path rises, smooth the baryon distribution and suppresses acoustic oscillations (called silk damping). The features of DM have a significant impact on the structure of the MPS. Because of the high baryon–photon interaction before recombination, if DM is made up of baryonic aggregates, the $P(k)$ would oscillate on small values of k. The lack of these kind of oscillations in observable data supports the hypothesis that DM is not made of baryons[30, 31].

From the history of the early universe, we observed that BBN, CMB, and MPS can be used as evidence for the presence of dark matter and can even anticipate its nature. They can also be used to constrain its interaction with the visible or invisible sector. Let us explore several other observable pieces of evidence that suggest the presence of dark matter.

1.1.4 Galactic rotation curve

According to the Kepler's law, the speed of orbits is proportional to the quantity of mass inside the orbit. With greater internal mass, the orbital speed increases. When mass is mostly concentrated in the center of the system, speed decreases with distance, as it does in the solar system i.e.,

$$v = \sqrt{\frac{GM}{r}} \tag{1.50}$$

The rotation curve of the galaxy should be comparable to the solar system if mass resides where the bright stuff is, however, measurements were not same as predicted. The missing mass problem reported by Fritz Zwicky, was disregarded for over four decades until Vera Rubin recorded velocity curves for edge-on spiral galaxies to previously unheard of precision in the late 1960s and early 1970s. She revealed that most stars in spiral galaxies circle the centre of the galaxies at around the same speed, which shows that the mass distribution throughout the galaxies was uniform even at the edge-on positions. The spiral galaxies were found to be embedded in a considerably bigger halo of unseen material ("dark matter halo"). The rotation curve can be seen in fig. 1.5 where the B curve shows the motion at edge-on galaxy and curve the A is according to the Kepler's laws [32].

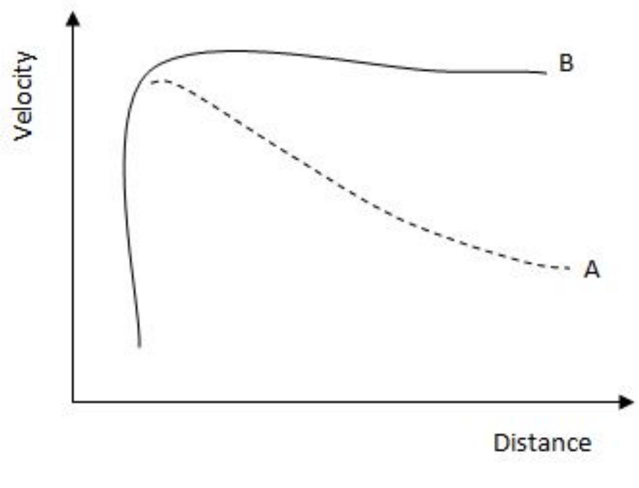

Figure 1.5: Galactic rotation curve.

1.1.5 Gravitational lensing

According to the general relativity, the existence of matter (energy density) may bend space-time, deflecting the course of a light beam. This phenomenon is known as gravitational lensing, and it is similar to the bending of light by lenses in optics in many ways. In 1997, Hubble space telescope image revealed gravitational lensing due to galaxy cluster. The foreground mass of the cluster is estimated to be about 250 times that of the observable matter in a cluster. The lensing is a completely non-dynamic way of detecting dark matter that depends on the impacts of general relativity to estimate masses.

When a big astronomical entity, such as a galaxy cluster, generates enough distortion of space-time for the trajectory of light that travels around it as if by a lens, gravitational lensing occurs. The observation of this distortion in geometry can help in determining the mass of the cluster that caused the anomaly. Weak gravitational lensing investigates minute distortions of galaxies induced by foreground objects in massive galaxy surveys using statistical analysis [33, 34].

The **Bullet Cluster** provides the most promising and direct observational evidence for dark matter till now. A collision between two galaxy clusters manifests in the Bullet Cluster [35], each of which is an ocean of blue dark matter with baryonic matter (in the form of $107 - 108$K gas, or plasma) sprinkling out inside. When gas particles encounter, they interact (electromagnetic interaction), get heated, and friction occurs, slowing them down and leaving them behind, while the dark matter does not interact with electromagnetic forces and continues to move as if nothing had occurred. As a result, the output of the computer simulation appears exactly like the image below.

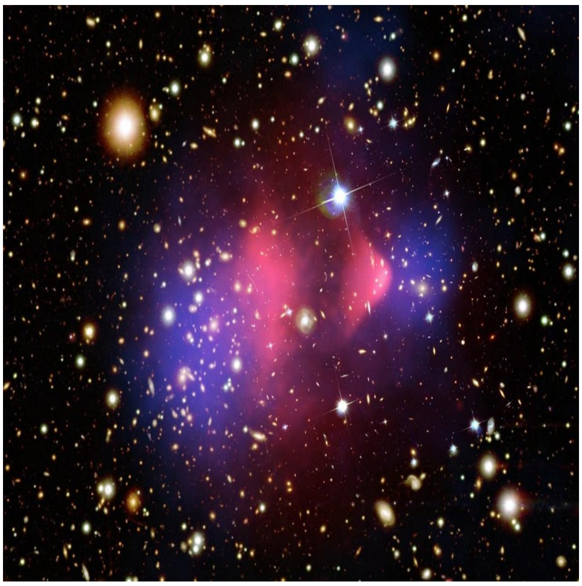

Figure 1.6: Bullet cluster [36].

Bullet Cluster is a shape that resembles a bullet. Unlike galaxy rotation curves, this dark matter evidence is believed to be direct proof of its existence because it is unaffected by Newtonian gravity specifics. This demonstrates that dark matter is the major source of gravity in all structures we can see, as well as it has very little interaction with the rest of the cosmos.

We have gone over the pieces of evidence for the existence of DM in this part. Every visible sector species has an appropriate particle candidate, in our SMPP. As a result, we would like to find a suitable DM candidate to make research easy. Let us look at some proposed DM candidate alternatives.

1.2 Various candidates for dark matter

Without dark matter, there would be no stars, galaxies, or humans. Still, we know very little about dark matter. What we know about the properties of dark matter, is listed as. It must be cold dark stuff moving slowly. It should also be electrically neutral as if it has an electric charge, we would be able to see it. It must live for atleast 13.8 billion years.

Not the obvious suspects, such as dead stars, black nebulae, and other faint objects that we could not see with a telescope. Because dark matter flows through each other in colliding bullet clusters, the scattering cross section might be used to constrain how DM interacts with itself. We know that dark matter should not interact more than a specific number of times based on the geometry of galaxies. As a result, dark matter is a minimally interacting entity with the rest of the universe. So, let us discuss other suggested alternatives for dark matter candidate.

1.2.1 MACHOs

Some stellar-sized objects that are extremely dark may not be observed directly with telescopes called Massive compact halo objects (MACHO). The notion of gravitational lensing is one way to look at them. We continue to track millions of stars in the Large Magellanic Cloud, a neighboring galaxy. These MACHOs may occasionally cross the line of sight of one of the stars in the Large Magellanic Cloud. It distorts space, bends light, and collects additional light by acting as a lens. MACHOs are not dark matter particles since they can only make up 10% of dark matter [37].

1.2.2 WIMP miracle

The word WIMP stands for weakly interacting massive particles. They interact with each other extremely weakly, even weaker than neutrinos. As a result, they are thought to be massive stable particles χ, formed in the early universe. WIMP interacts with gravity as well as with any other force which is weaker than weak nuclear force with non-vanishing interaction strength. It is expected that most of the WIMP candidates are thermally produced in the early universe, similar to the particles of the SM according to Big Bang cosmology, and they will usually constitute cold dark matter today via thermal production requires a self-annihilation cross-section of $\langle \sigma \upsilon \rangle \simeq 3 \times 10^{-26} \mathrm{cm}^3\mathrm{s}^{-1}$ in the early universe, which is appropriate for a new particle with a mass of 100GeV that interacts through the electroweak force [33]. This seeming synchronicity is known as the WIMP miracle since supersymmetric extensions of the SMPP predict a new particle with similar properties, and a stable super symmetric partner has long been a top WIMP candidate.

We acquired an understanding of the nature of DM by studying cosmological observations. To detect DM, cosmologists and physicists used a variety of direct, indirect, and collider experiments. So, in the next section, we will talk about the current status of the DM search.

1.3 Current status of DM search

Because WIMP searches are the most common sort of dark-matter candidate, they will be discussed here (or at least the type that receives the most experiments).

The three basic methods for identifying dark matter particles are: direct detection, producing them in accelerators (collider searches), and indirect detection. Let's talk about them in the next parts.

1.3.1 The search for DM using the Collider

Because WIMPs are neutral and weakly interact, they will not be directly detected if they are formed at colliders like Large Hadron Collider (LHC). The LHC is actively aiming to synthesize DM through high-energy proton beam collisions. Because WIMPs belong to theories outside the realm of the Standard Model, quarks and gluons in protons crushed together at the LHC often do not annihilate directly to WIMPs but they may annihilate to a range of various additional particles. When trying to reconstruct the chain of events, those additional particles might decay to WIMPs inside the detector, leaving a signal of missing energy. But there is no signature of DM particle at LHC [38].

1.3.2 The search of DM using the direct detection methods

The discovery of WIMPs from our Galactic halo as they pass through and past the Earth might be a solution to the dark matter dilemma. This would also allow for the determination of dark matter's local density, proving beyond a shadow of a doubt that it is non-baryonic cold dark matter. As we have a general idea of the speed ($\sim$ 220km s^{-1}) and the density ($\rho \sim 0.3$ proton masses cm^{-3}), we can estimate that about 100000 dark matter particles per second travel through every square centimeter of the Earth for a WIMP with a mass of 10–100GeV. However, if WIMPs exist, they are very weakly interacting particles, so it is quite rare that one of them will interact at all, and the rest of the particles pass right through the Earth without any interaction. In addition, if a WIMP undergoes elastic scattering with nucleus, the deposited energy is usually in the 1keV to 100keV range, which is too small to be detected except by exquisitely sensitive equipment. Despite these challenges, several organizations across the world are working on building equipment that can detect WIMPs. The detection rates are within and barely beyond the capabilities of existing experimental efforts.

So, the key focus is to detect the modest amount of energy deposited when a WIMP undergoes scattering with a nucleus in a well-instrumented medium. Due to scattering it recoils, produce randomness in the structure, crystal lattice vibrations (such as phonon or heat), and ionization. These signals are observable. Another option is to utilize noble liquid detectors like liquid xenon or argon, which detect the scintillation light produced due to particles collision. These tests are conducted deep below to ignore the impact of ionizing cosmic rays and detectors are normally operated at extremely low temperatures to reduce thermal excitations. Shielding in a variety of forms, as well as redundant detection systems, are becoming more widespread. Regardless, these are difficult examinations, and even little amounts of radioactivity in the detector can dominate the intended signal.

Two methods exist for distinguishing the events from the background. Background impact can be detected and disregarded in some detectors. But in most of the detectors, it is hard to detect the background impact, so they rely on the knowledge that the WIMP event rate is expected to be higher in June than it is in December as the orbit of the Earth is either aligned with the motion of the Sun in Galaxy (in June and December respectively), which causes this yearly modulation in event rate. Detection thresholds for the modern scenario of detectors are about 1 event $\text{kg}^{-1}\text{day}^{-1}$, with the aim that signals as tiny as 10^{-2} events $\text{kg}^{-1}\text{day}^{-1}$ will be detectable within the next few years.

CDMS, CRESST, and EDELWEISS are examples of cryogenic detector experiments that use the recoil approach. ZEPLIN and XENON are examples of noble liquids. DAMA/NaI, and DAMA/LIBRA are two further trials worth mentioning. Here, we look only for XENON experiment for DM search [39].

XENON Experiment

In order to find dark matter, the XENON experiment looks for unexpected interactions in a liquid xenon target. The target volume is positioned within the time projection chamber (TPC), which is a dual-phase liquid Xenon time projection chamber (LXeTPC) with a high electric field.

Both ionization via proportional scintillation in the Xe gas phase (S2) and direct scintillation light (S1) in the liquid Xe are detected with the help of two arrays of photo-multipliers (PMT) below and above the field. Between the upper end of the TPC and the top PMT array, the liquid-gas border lies. The value of the ratio of two signals, S1/S2 is different for electron and nuclear events, so it offers a strategy to detect the background impact.

The XENON collaboration released a remarkable conclusion from their attempt for dark matter detection, in 2020. The Gran Sasso Laboratory in Italy studied data obtained with the XENON100 detector over the period of 13 months of operation and found no sign of WIMPs. Two of the detected events are statistically compatible with one event that arise due to the background radiation. The world-leading sensitivity has been enhanced by a factor ~ 3.5 when compared with their previous performance. This tightens the constraints even more on models with WIMP candidates and therefore makes future WIMP searches easy [40].

1.3.3 Detection via Indirect Means

Another potential approach for WIMP detection has been the subject of a lot of theoretical and practical work. If dark matter particles are WIMPs, they have been moving between the Sun and the Earth for billions of years. So, elastic scattering of WIMP with nuclei in the Sun or Earth causes loss in their energy or alters their direction to get caught in the gravitational pull of the Sun or Earth. The trapped WIMPs' orbits will continue to traverse the Sun (or Earth), and eventually, settle the WIMPs into the core. The self-annihilation rate will rise as the number density rises over time. Ordinary neutrinos can be produced by WIMP self-annihilation, hence a flux of neutrinos from the Sun or Earth's core is expected. Neutrinos are easily ejected from the solar core. Gamma rays, positrons, and antiprotons can also be produced by the WIMP annihilation.

Fermi-Gamma Ray Space Telescope

The Fermi Gamma-Ray Space Telescope (FGST), which was launched on June 11, 2008, is looking for gamma rays produced by dark matter annihilation and decay. Since its launch, the Fermi satellite's Large Area Telescope (LAT) has been looking for this "annihilation signature". We have not seen this signal yet because it is not as easy as pointing Fermi towards the greatest dark matter cluster and hoping for the best. Although the galactic center is a good area to look for an annihilation signature, it contains a several number of fascinating and gamma-ray generating objects. So, dwarf spheroidal satellites orbiting the Milky Way are another option. But their gravity is really not powerful enough to keep them in for long, most of the stars on these little satellites have been stripped away, but the dark matter has remained mostly intact. As a result, we should witness a weaker dark matter signal originating from these cores which would be less hidden and less confused by other baryonic sources. A few observational claims linked to the dark matter particles have been reported, but none of them has received widespread support. Yet, searches have shown no conclusive evidence of DM production [41].

1.4 Thesis Outline

The main goal of this thesis is to look at the underlying characteristics of the DM, namely its non-gravitational interactions with itself and other particles.

We have reviewed various aspects of DM in this introductory chapter, including its cosmological evidences with a detailed discussion of three of the most crucial epochs from the chronology of the early universe, suggested alternatives, and collider, direct, and indirect searches of DM.

The non-gravitational interaction of DM with the visible sector is the subject of Chapter 2. We use the interaction between DM and neutrinos for this. Then, using perturbation equations for this interaction in the CLASS code, we examine the impact of this interaction on cosmological observations like CMB, polarisation, and MPS. We answer the long-standing problem of Hubble tension by reconciling the effects of this interaction with respect to the ΛCDM model. By imposing strict limitations on the cosmic parameters, we may more precisely limit the models for such interactions.

At last, we provide our conclusion of this thesis.

Chapter 2

Constraints on dark matter and neutrino interaction

2.1 Introduction

In ΛCDM Model, the dark matter is assumed to be consist of collision-less and non-relativistic particles. However, various particle physics models consider non-gravitational interaction between DM and SM particles (ex. ν, photons, baryons etc). In some PP models dark matter interacts with the dark sector (ex. dark radiation). Such types of interactions are expected in the WIMP paradigm and several extensions of the SM. Because it suppresses primordial density fluctuations and erases structures with a scale lower than the collisional damping scale, DM interaction beyond gravity leaves a visible trace on the CMB and matter power spectrum. In this part, we discuss DM-ν interaction (DNI). We take DM-ν interaction in late the universe so that it does not affect the history of the early universe, i.e., this interaction will take place when neutrinos will be non-relativistic ($z \approx 100$).

The CMB data from the Planck satellite is used to constrain the DM-ν interaction. To exclude nuisance factors representing foregrounds and instrumental effects, we use both the low and high multipole data. The Planck collaboration's measurement of the CMB lensing potential power spectrum is also used. Baryon acoustic oscillation data from Baryon Oscillation Spectroscopic Survey (BOSS) [42], Galaxy clustering surveys [43], WiggleZ [44], etc., check the validity of ΛCDM model. While CMB experiments like Planck allow for precisely constraining the cosmic parameters, the matter power spectrum ($P(k)$), due to its extraordinary accuracy, can be a key for the information on the DM particle characteristics.

This is how the chapter is laid up. In section [2.2], the altered perturbation equations are demonstrated that include the DM-ν interaction and describe the implementation of these equations in Boltzmann code, CLASS [23]. In section [2.3], we show the effects of DM-ν interaction on the CMB (in section [2.3.1]) and the MPS (in section [2.3.2]). In section [2.4], we present the effect of the Hubble parameter on these spectra. Here our work is model-independent. In section [2.5], we give the conclusion.

2.2 Implementation of perturbation equation

Perturbation equations[1] in conformal Newtonian gauge, in presence of DM-ν interaction, can be given as

$$\begin{aligned}
\dot{\delta}_{\mathrm{DM}} =& -\theta_{\mathrm{DM}} + 3\dot{\phi}, && (2.1)\\
\dot{\theta}_{\mathrm{DM}} =& -\frac{\dot{a}}{a}\theta_{\mathrm{DM}} + k^2\psi - \left(\frac{4\rho}{3\rho_{\mathrm{DM}}}\right)\dot{\mu}(\theta_{\mathrm{DM}} - \theta_\nu), && (2.2)\\
\dot{\delta}_\nu =& -\frac{4}{3}\theta_\nu + 4\dot{\phi}, && (2.3)\\
\dot{\theta}_\nu =& k^2\left(\frac{1}{4}\delta_\nu - \sigma_\nu\right)\theta_{\mathrm{DM}} + k^2\psi - \left(\frac{4\rho}{3\rho_{\mathrm{DM}}}\right)\dot{\mu}(\theta_{\mathrm{DM}} - \theta_\nu), && (2.4)\\
\dot{F}_{\nu 2} =& 2\dot{\sigma}_\nu = \frac{8}{15}\theta_\nu - \frac{3}{5}kF_{\nu 3} - \frac{9}{5}\dot{\mu}\sigma_\nu, && (2.5)\\
\dot{F}_{\nu l} =& \frac{k}{(2l+1)}[lF_{\nu\ l-1} - (l+1)F_{\nu\ l+1}] - \dot{\mu}F_{\nu l}, \qquad l \geq 3. && (2.6)
\end{aligned}$$

Here, the comoving wave number is k, dots show the derivatives over the conformal time, ψ and ϕ are the Newtonian potentials, θ_ν and θ_{DM} are the neutrinos and DM velocity divergences, density perturbations of neutrino and DM are δ_ν and δ_{DM}, σ_ν is the neutrino anisotropic stress potential, $F_{\nu l}$ is the higher ($l \geq 3$) neutrino moment and $\mathcal{H} = \left(\frac{\dot{a}}{a}\right)$ is the conformal Hubble parameter. For more detail, one can look at Appendix [A].
The differential optical path or DM-ν interaction rate can be written as

$$\dot{\mu} = an_{\mathrm{DM}}\sigma_{\mathrm{DM}-\nu}. \tag{2.7}$$

Here, $\sigma_{\mathrm{DM}-\nu}$ is the elastic scattering cross-section of the DM-ν interaction, n denotes the DM number density which is given as $n_{\mathrm{DM}} = \rho_{\mathrm{DM}}/m_{\mathrm{DM}}$, ρ_{DM} is the energy density of DM and m_{DM} is the mass of DM.
The impact of the DM-ν interaction on the evolution of primordial density fluctuations may be quantified by using the dimensionless variable

$$u = \left[\frac{\sigma_{\mathrm{DM}-\nu}}{\sigma_{\mathrm{Th}}}\right]\left[\frac{m_{\mathrm{DM}}}{100\mathrm{GeV}}\right]^{-1}, \tag{2.8}$$

here, the Thompson scattering cross-section is, $\sigma_{Th} = 6.65 \times 10^{-25}\mathrm{cm}^2$. The effective suppression at small-scale is determined by the interaction cross-section to DM mass ratio, because the size of the parameter defines the collisional damping scale.

[1]All necessary modifications in CLASS code are confined in the perturbation and thermodynamics modules.

In most of the models of the particle physics, the DM-ν interaction cross-section might have one of the two unique behaviours: it will either be constant or will depend on temperature as T^2. For those models in which cross-section depends on T^2, $u(a)$ will be $u(a) = u_0 a^{-2}$, here u_0 is the present-day value [45, 46].

2.3 Results from cosmological observation

We take a flat ΛCDM model (where the parameters are taken from Planck data) into account with the only additional coupling of DM and neutrino. Here, we consider interaction cross-section as a constant for simplicity. The temperature-dependent cases show similar impacts. In this part, we discuss the impact of the DM-ν interaction on the CMB angular power spectrum [sec. 2.3.1] and matter power spectrum [sec. 2.3.2] for constant elastic scattering cross-section, with the help of the modified CLASS code (modifications are mentioned in [sec. 2.2]).

2.3.1 Cosmic Microwave Background

Despite accumulation under gravitational force as for ΛCDM ($u = 0$), DM perturbation receives collisional damping after entering the horizon. As a result, density fluctuations of the DM are suppressed, resulting in shift and change in amplitudes of peaks. For varying value of parameter u, the influence of DM-ν interactions may be observed on the CMB angular power spectrum's EE and TT components in fig. 2.1, and for BB component in fig. 2.3.

In the TT and EE components of the CMB spectrum, we may see a little shift towards higher l and an increase in peaks when compared to the ΛCDM model, which can be interpreted as follows.

Physics behind the change in peaks of TT and EE components of CMB for DM-ν interaction:

- The gravitational force experienced by the baryon-photon fluid before decoupling determines the geometry of the CMB peaks. DM-ν interaction resists free streaming of neutrinos, resulting in the accumulation of neutrinos. This gives a boost to the gravitational influence in the integrated Sachs-Wolfe effect. So, this results an enhancement in peaks.

- In DM-ν interaction, DM and neutrinos behave like a fluid. So, its effective sound speed is given as $c^2_{\mathrm{DM}-\nu} = [3(1 + 3\rho_{\mathrm{DM}}/\rho_\nu)]^{-1}$. Since $\rho_{\mathrm{DM}}/\rho_\nu$, ratio is very large, so this fluid has a smaller sound speed in comparison to photon-baryon fluid. Due to this, wavelength of photon-baryon fluid is larger than the DM-ν fluid. So, there is a shift in peaks towards higher l.

- In DM-ν interaction, modes which are at higher l have higher phase shift compared to those which are at lower l since at later time density contribution of neutrinos compared to matter density contribution decreases in the matter dominated era. This relative density distribution for neutrinos can be given as, $\rho_\nu/(\rho_r + \rho_m)$. Here, ρ_r is the distribution of radiation energy density and ρ_m is DM energy density distribution. This effect can be seen in fig. 2.2.

- Damping tail of the CMB spectrum is a signature of diffusion damping. Because diffusion greatly suppresses peaks at the damping tail, there is no discernible difference between standard and non-standard damping tails.

- The late integrated Sachs-Wolfe effect dominates the CMB spectrum at small values of l. So for the DM-ν interaction, this part of the spectrum is not much affected. So, there is no visible difference in the standard and non-standard Sachs-Wolfe part of the CMB spectrum [46, 47].

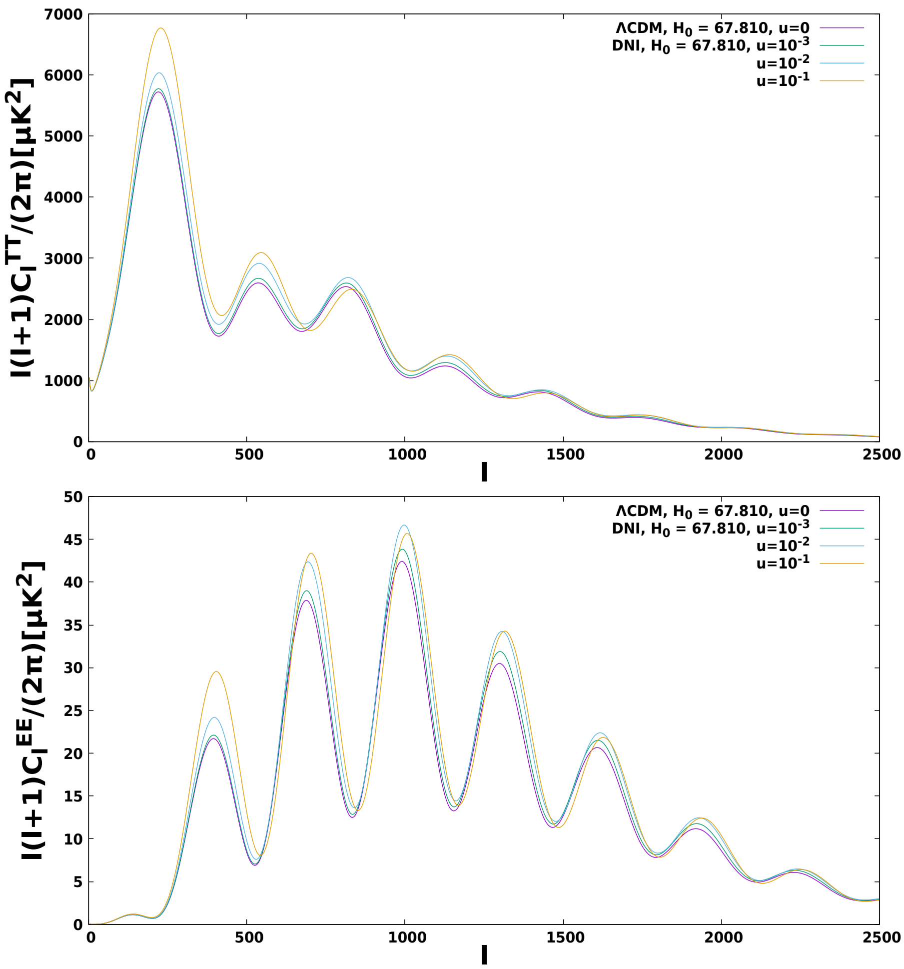

Figure 2.1: The impact of DM-ν interaction on the TT component of the angular power spectrum (upper part), EE component of the angular power spectrum (bottom part).

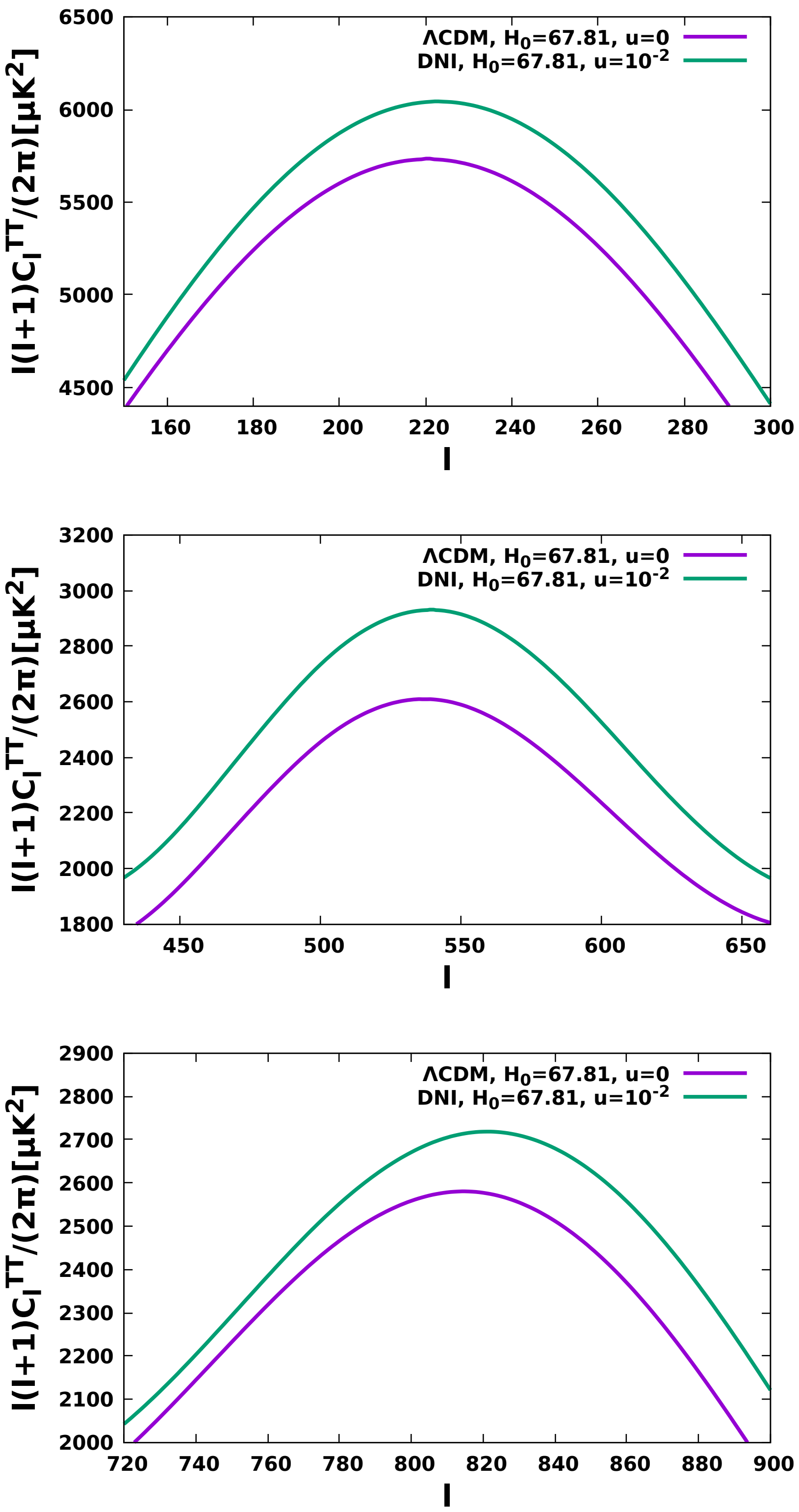

Figure 2.2: A clear visibility of an enhancement and shift in different peaks of TT component of CMB spectrum towards higher l due to DM-ν interaction ($u = 0.01$) in comparison to ΛCDM model ($u = 0$).

Physics behind the change in peaks of BB components of CMB for DM-ν interaction:

The TT component of CMB angular spectrum is a thermal signal that can be perturbed by other astrophysical sources like integrated-Sachs-Wolfe effect. So, to check the validity of a model we look for BB component of CMB as these modes are only produced by gravitational waves.

The effect of dark matter and neutrino interaction on BB-modes can be seen in fig. 2.3.

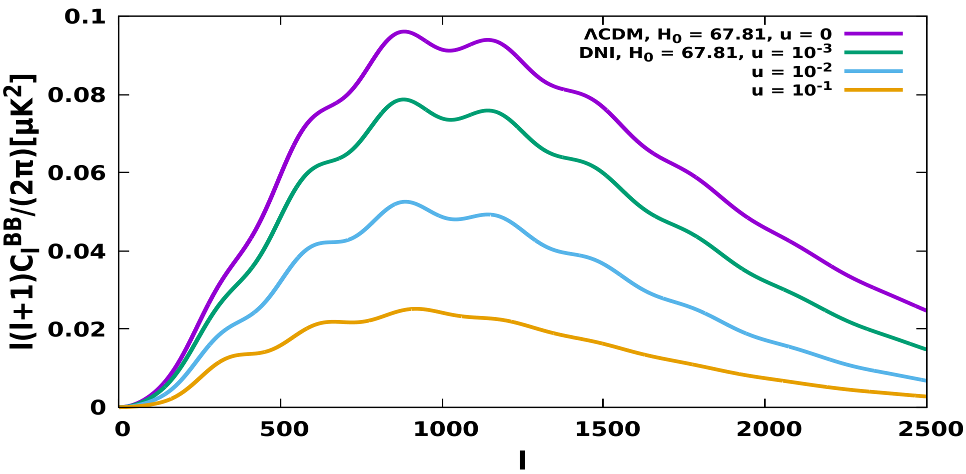

Figure 2.3: The impact of DM-ν interaction on the BB component of the angular power spectrum.

Collisional damping in the perturbation of the DM density, causes the suppression of peaks for the DM-ν interaction as compared to the ΛCDM model. Since these modes are produced due to gravitational waves, accurate measurements of the B-mode signal may be used to investigate alternative inflationary scenarios. But there is no compelling evidence for B-modes due to the limited amplitude of the CMB polarization signal in comparison to temperature anisotropies [48].

2.3.2 Matter Power Spectrum

DM-ν interaction produces a series of damped oscillations at small scales or large wave-number (k) values, similar to Dark Acoustic Oscillations[2] (DAO) [49] that can be seen in fig. 2.4.

To explain the physics behind the damped oscillations at small scales, let us discuss about the origin of oscillations. Oscillations in matter power spectrum for

[2]Dark Acoustic Oscillations (DAO)→ When DM atom is coupled to dark radiation non-gravitationally, this interaction prohibits DM to form gravitationally bound structure. If DM decouples from the coupled particles at late time, then its impact can seen on matter power spectrum at large scale in terms of dark acoustic oscillations, in a similar way to BAO.

DM-ν interaction arise because DM fluid attains a non-zero pressure due to its interaction with neutrinos before recombination. Now, let us discuss about the damping of the oscillations. The physical damping phenomena known as mixed damping occurs when dark matter is kinetically connected to another species that are free flowing. So, dark matter perturbations are damped by the mixed damping effect, which is a combination of collisional and free-streaming damping. For larger value of DM-ν interaction strength (u), collisional damping takes place and for smaller value of u, free-streaming damping takes place [46, 47, 50, 51].

Let $\Gamma_{\nu-\mathrm{DM}} = n_{\mathrm{DM}}\sigma_{\nu-\mathrm{DM}}$ is the neutrino interaction rate with DM with $\sigma_{\nu-\mathrm{DM}}$ cross-section and $\Gamma_{\mathrm{DM}-\nu} = n_\nu\sigma_{\nu-\mathrm{DM}}$ is the DM interaction rate with neutrino. Here, $\Gamma_{\nu-\mathrm{DM}} \neq \Gamma_{\mathrm{DM}-\nu}$ because $n_{\mathrm{DM}} \neq n_\nu$. Thus, for mixed damping to take place, the below conditions must be fulfilled [52] i.e.,

$$\Gamma_{\mathrm{DM}-\nu} > H > \Gamma_\nu = \Gamma_{\nu-e^-} + \Gamma_{\nu-\mathrm{DM}}.$$

Here,

$$\Gamma_{\nu-\mathrm{DM}} = n_{\mathrm{DM}}\sigma_{\nu-\mathrm{DM}}$$

and

$$\Gamma_{\mathrm{DM}-\nu} = \frac{4\rho_\nu}{3\rho_{\mathrm{DM}}}\Gamma_{\nu-\mathrm{DM}}.$$

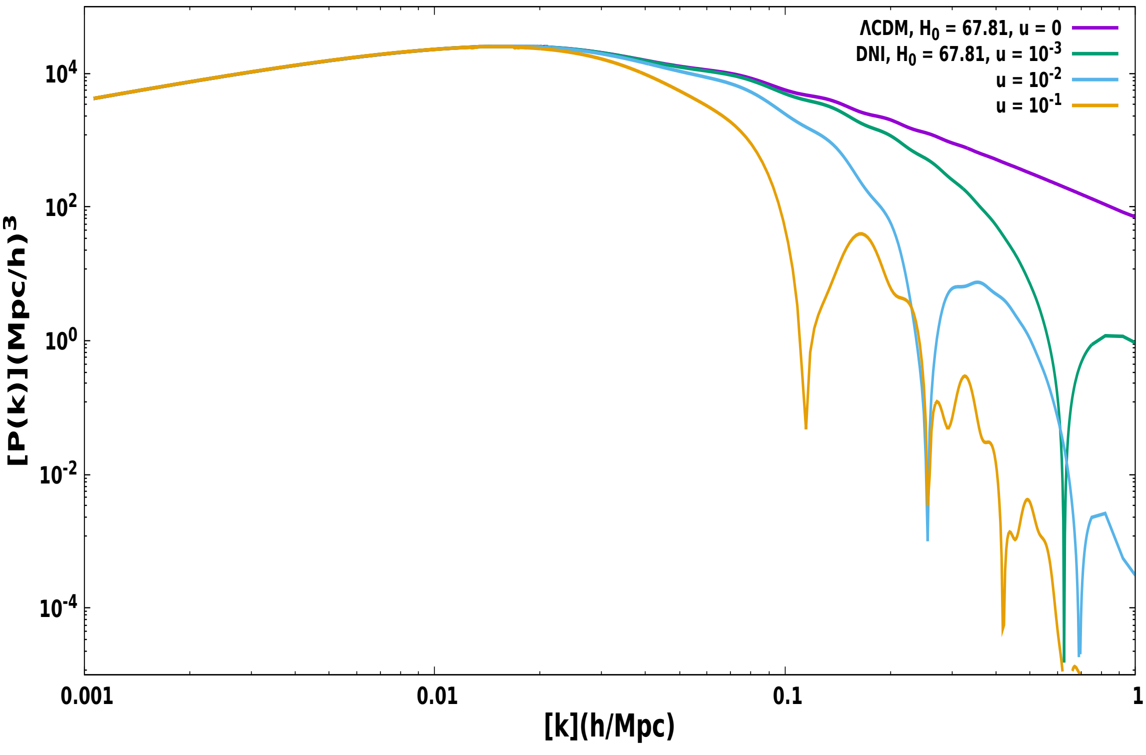

Figure 2.4: The change in the matter power spectrum with different values of DM-ν interaction strength (u). This shows a suppression of structure formation at large wave-numbers (k) with an increment in value of u.

Fractional change between standard matter power spectrum and non-standard matter power spectrum for strength $u = 10^{-1}$ of DM-ν interaction, can be seen in fig. 2.5.

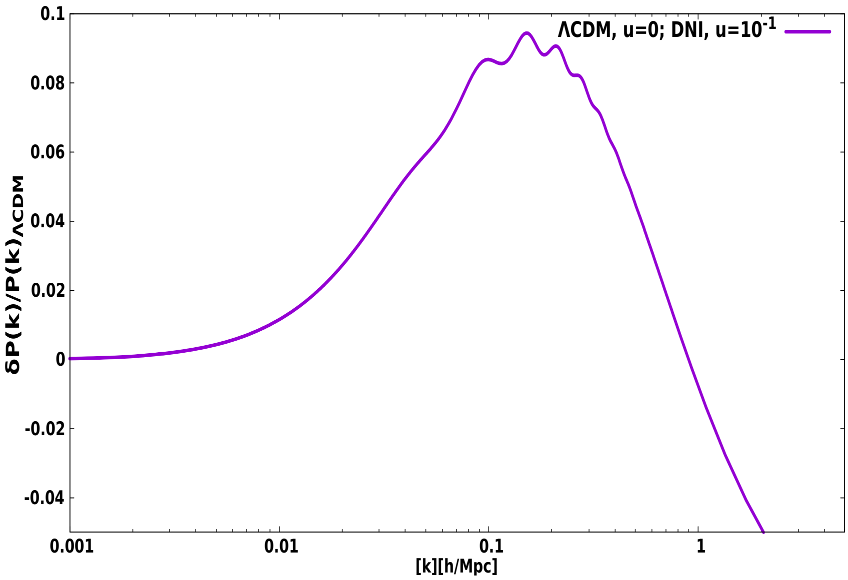

Figure 2.5: The fractional change in the matter power spectrum with DNI ($u = 0.1$) in comparison to the standard matter power spectrum with $u = 0$.

Let us discuss about the constraints on matter power spectrum put by the Lyman-α forest data [46, 53].

Constraints from the Lyman-α forest

The Lyman-α absorption is produced by the intergalactic neutral hydrogen in the spectra of distant quasars, so named as "Lyman-α forest". It is a powerful tool for limiting dark matter properties, notably the free-streaming of warm dark matter particles (WDM).

In general, suppression in matter power spectrum at small scale is described by a transfer function $T(k)$ as

$$P(k) = T^2(k) P_{\rm CDM}(k).$$

Here, $P_{\rm CDM}(k)$ denotes the matter power spectrum of ΛCDM. For non interacting WDM, transfer function is given as

$$T(k) = [1 + (\alpha k)^{2v}]^{-5/v},$$

with
$$\alpha = \frac{0.049}{\rm h\ Mpc^{-1}} \left(\frac{\rm m_{WDM}}{\rm keV}\right)^{-1.11} \left(\frac{\Omega_{\rm DM}}{0.25}\right)^{0.11} \left(\frac{h}{0.7}\right)^{1.22}.$$

Here, $v \approx 1.12$, mass of the WDM is given by $m_{\rm WDM}$, and $h = H_0/100{\rm kms}^{-1}{\rm Mpc}^{-1}$, is the Hubble constant.

The constraints on the free streaming of WDM are derived from an analysis of the Lyman-α flux measured by the Keck High Resolution Echelle Spectrometer (HIRES) [54] and the Magellan Inamori Kyocera Echelle (MIKE) spectrograph [55]. The basic property of WDM that affect matter power spectrum is its thermal velocity. Thus, free-streaming of WDM eliminate density fluctuations on scale below a particular comoving wave-number which is given as

$$k \sim 15.6 \frac{h}{\rm Mpc} \left(\frac{m_{\rm WDM}}{1{\rm keV}}\right)^{4/3} \left(\frac{0.12}{\Omega_{\rm DM}h^2}\right)^{1/3}.$$

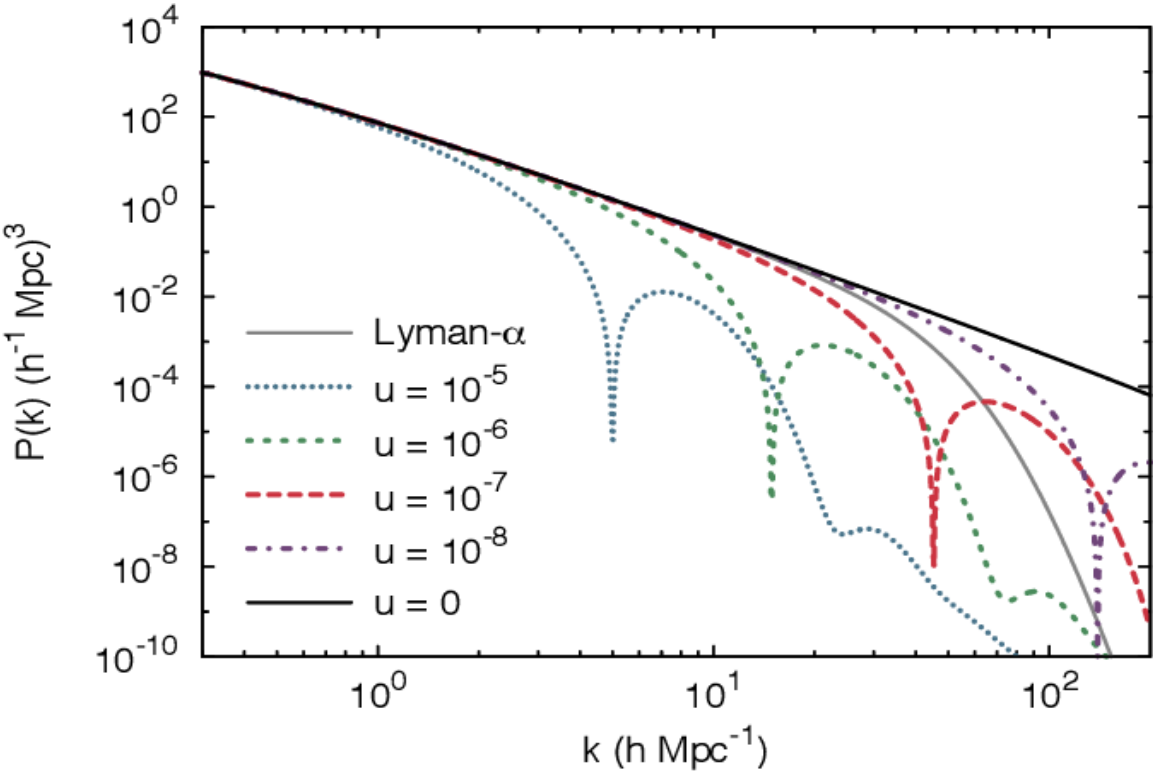

Figure 2.6: The curve with $u = 0$ represents the matter power spectrum for ΛCDM (without DM-ν interaction), curves with $u \neq 0$ represent the impact of DM-ν interaction on matter power spectrum, and the grey curve (titled as Lyman-α) represents the most recent constraint on warm dark matter or interacting dark matter from the Lyman-α forest [46].

From fig. 2.6, by comparing matter power spectrum for DM$-\nu$ interaction with matter power spectrum from Lyman-α forest data, we can effectively rule out those DM-ν interactions for which collisional damping scale is larger than the maximally allowed WDM free-streaming scale.

DM-ν interaction resolves one of the longest standing problems named as the Hubble tension. Let us discuss the relaxation in the Hubble tension using DNI and the constraints on DM-ν interaction parameters.

2.4 Undoing neutrino phase-shift

The position of the peaks in the TT component of the CMB spectrum is approximately around the maximum cosine function, $\cos(kr_s + \phi)$. Here, k is the comoving wave number, ϕ is the phase shift due to free-streaming neutrinos and r_s is the comoving sound horizon at recombination. So, position the peaks can be given by $kr_s = m\pi - \phi$ at particular k, here $m \geq 1$, an integer. And for particular k, there will be a particular multipole (l) which can be given as

$$l_{\text{peak}} \approx k_{\text{peak}} = (m\pi - \phi)\frac{D_A}{r_s}, \tag{2.9}$$

$$\text{where} \quad D_A = \int_0^{z_s} dz \frac{1}{H(z)}, \qquad r_s = \int_{z_s}^{\infty} dz \frac{c_s(z)}{H(z)}. \tag{2.10}$$

Here, $H(z)$ is the Hubble parameter, D_A is the comoving angular diameter distance at recombination, and $c_s(z)$ is the effective speed of sound for baryon-photon fluid. From point 1 of section [2.3.1] we got to know that the gravitational effect gets a boost due to DM-ν interaction and due to this angular diameter changes. As angular scale depends of angular diameter distance, peaks position also changes. In fig 2.1 and 2.2 of section [2.3.1], we can see that there is a phase shift due to DM-ν interaction. Hence to fix peaks position at particular l, we need to fix angular diameter distance which can be fixed by changing the Hubble parameter value. But history of the early universe depends of sound horizon distance (r_s) which also depends on Hubble parameter value. So, we need to change H such that it does not affect r_s. Hence a change in $H^2(z) \to H^2(0) + \delta H^2(0)$, is only significant at low red-shift z, and thus has a negligible impact on r_s. Increasing the Hubble parameter produces a negative phase shift which increases with m.

We can use this feature of the Hubble parameter to solve one among the most prevalent issues between astrophysical and cosmological observations which is known as **Hubble tension** [46, 47, 56, 57, 50]. It is the distinction between the Hubble parameter values as measured by CMB and local observations. We can see the Hubble values obtained from different observations in fig. 2.7.

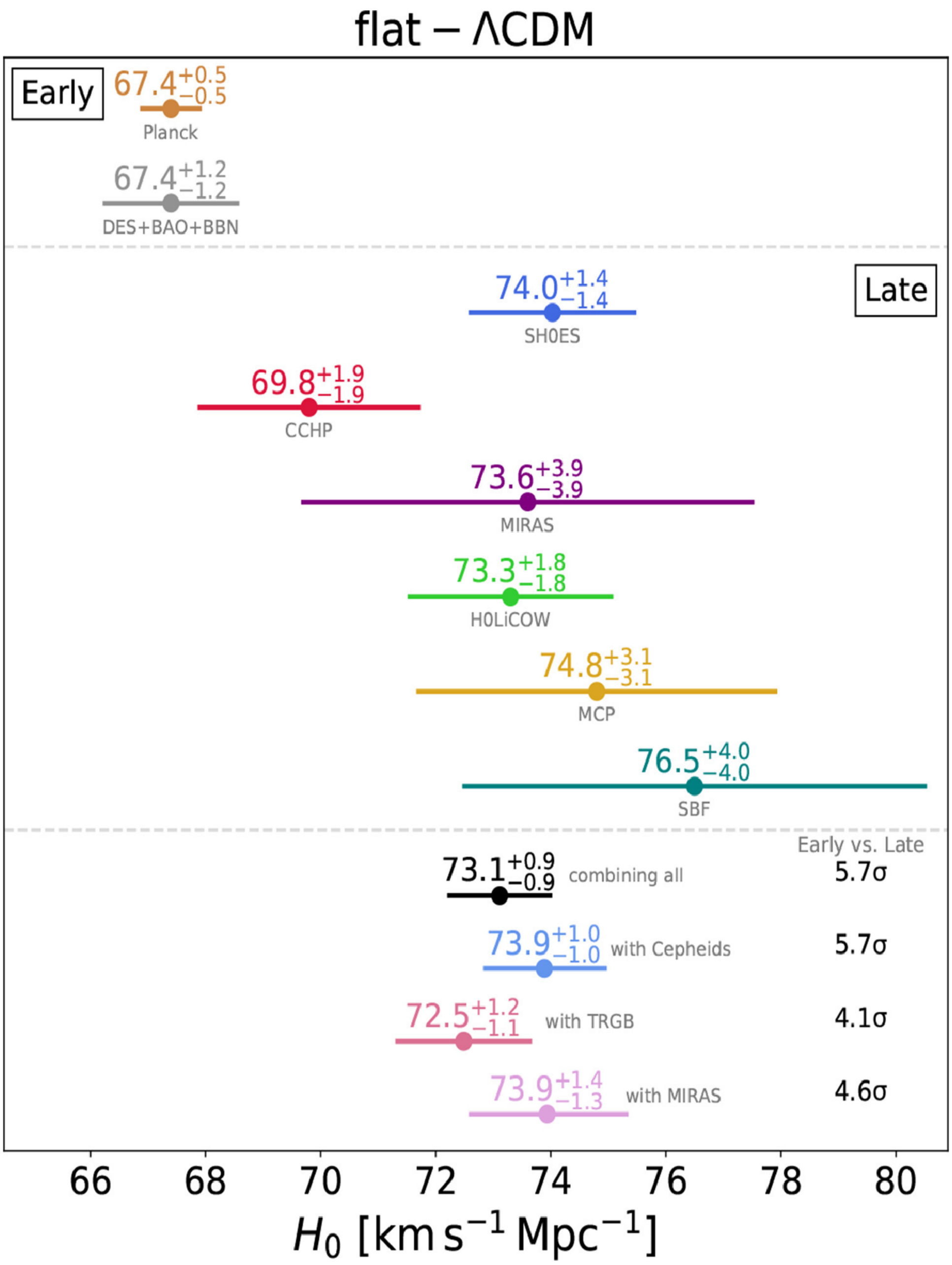

Figure 2.7: Two independent predictions for H based on early-Universe data (Planck Collaboration. 2018; Abbott. 2018) are shown at the top panel, while the middle one shows measurements of the late universe. And the bottom panel shows combinations of measurements of the late universe and the tension in comparison to the early universe predictions [58].

Standard ΛCDM cosmology or CMB gives the Hubble parameter value as $H_0 = 67.5 \pm 0.6 \mathrm{kms}^{-1}\mathrm{Mpc}^{-1}$ [59], Hubble Space Telescope (HST) observation gives $H_0 = 74.03 \pm 1.42 \mathrm{kms}^{-1}$ Mpc^{-1} [60]. There is $\approx 4.1\sigma$ discrepancy between these two values. Improved analysis in both the early universe and late universe observations has been unable to reduce this gap. Therefore, by opening the space for DM-ν interaction and increasing the Hubble parameter value to readjust the shift in peaks in comparison to ΛCDM model, helps us to reduce the Hubble tension upto 2σ with an upper limit on DM-ν interaction strength, 0.034 [50]. The impact of increased the Hubble value with DM-ν interaction can be seen in fig. 2.8.
A clear view of the impact of the DM-ν interaction at different Hubble values corresponding to the standard cosmology spectrum can be seen at different peaks in fig. 2.9.
This cosmological observation can be seen as a hint for shaping physics beyond the Standard Model. By adjusting the rest of the parameters of CMB, we can bring back peaks height to its original size. List of the best-fit parameters for DNI cosmology is given in Table. 2.1 that reconcile the effect produced by dark matter and neutrino interaction, in comparison to ΛCDM model.

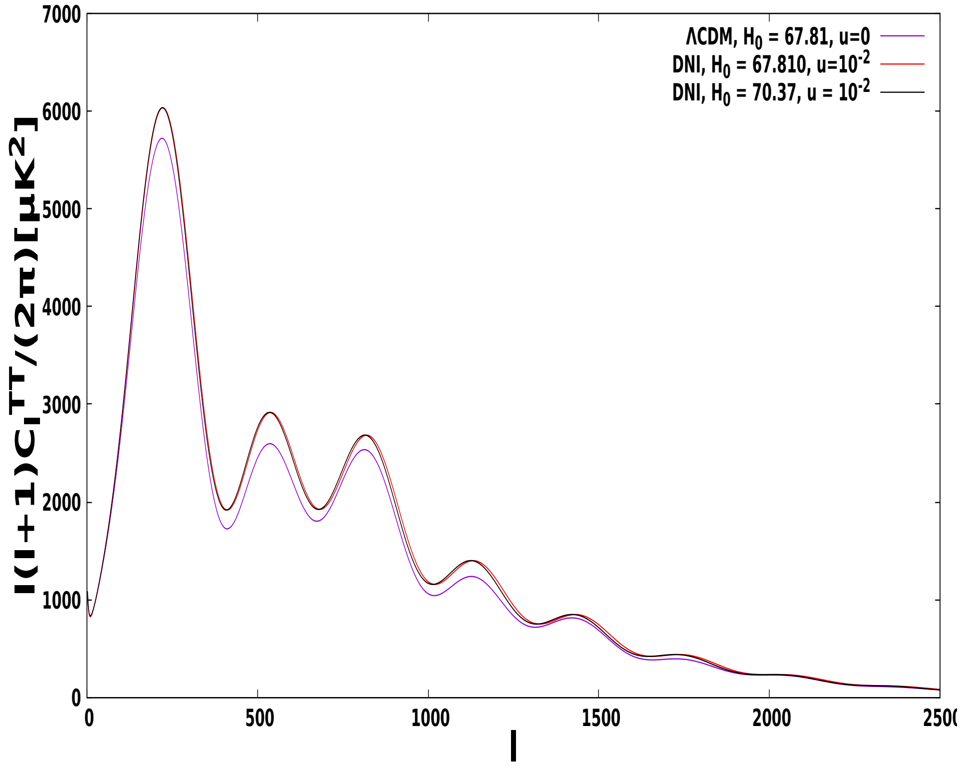

Figure 2.8: TT power spectrum for CMB and DM-ν interaction with strength $u = 10^{-2}$ at different values of Hubble parameter.

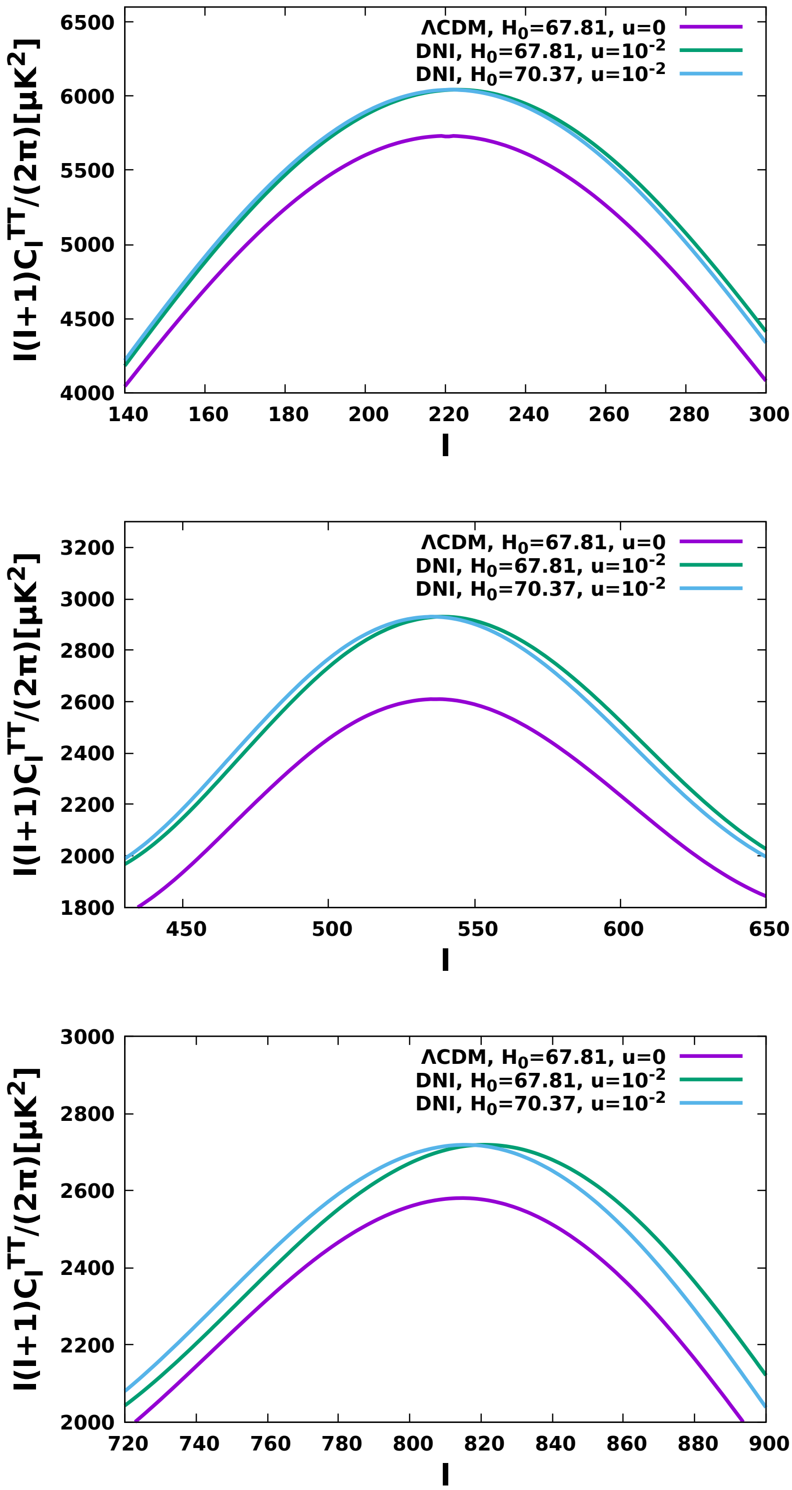

Figure 2.9: The impact of the DM-ν interaction at different Hubble values corresponding to CMB can be seen at three different peaks. DM-ν interaction with increased Hubble value brings back peaks to their original positions.

Name of the parameter	ΛCDM model (Planck 2018 dataset)	DNI model
H_0 (Hubble parameter)	67.3 ± 1.2 (67.81) $\mathrm{kms^{-1}Mpc^{-1}}$	69.5 ± 1.2 (70.37) $\mathrm{kms^{-1}Mpc^{-1}}$
u (DNI strength)	0	$\sim 10^{-2}$
$100\Omega_b h^2$ (baryon density$=\rho_b/\rho_c$)	2.205 ± 0.028	2.2250 ± 0.029
$\Omega_{\rm DM} h^2$ (baryon density$=\rho_{\rm DM}/\rho_c$)	0.1199 ± 0.0027	0.1256 ± 0.0055
n_s (scalar spectral index)	0.9603 ± 0.0073	0.9330 ± 0.0104
$\ln 10^{10} A_s$ (amplitude)	2.196 ± 0.051	2.020 ± 0.063
$\mathrm{N_{eff}}$ (neutrino flavour)	3.046000 ± 00	3.046000 ± 00
$z_{\rm reio}$ (reionization redshift)	11.1 ± 1.1	10.8 ± 1.1
$100\theta_s$ (angular scale)	1.0411 ± 0.0003	1.0411 ± 0.0003

Table 2.1: Table of best-fit parameters for the DNI (DM-ν interaction) cosmology, that reconcile the impact of DM-ν interaction in comparison to ΛCDM model [46].

This tension can be further reduced to some level by opening parameter space for $N_{\rm eff}$.

Let us discuss how $N_{\rm eff}$ will affect angular power spectrum. The energy density for relativistic particles is given as

$$\rho_r = \rho_\gamma \left[1 + \frac{7}{8}\left(\frac{4}{11}\right)^{\frac{4}{3}} N_{\rm eff}\right]. \tag{2.11}$$

And the Hubble parameter is given as,

$$H(z) = H_0\sqrt{(\Omega_{\rm DM} + \Omega_b)(1+z)^3 + \Omega_r(1+z)^4} \tag{2.12}$$

$$= H_0\sqrt{(\Omega_{\rm DM} + \Omega_b)(1+z)^3 + \Omega_\gamma(1+z)^4(1 + 0.2271 N_{\rm eff})}. \tag{2.13}$$

In equation (2.12), we have used equation (2.11). From equation (2.10) we have,

$$D_A = \int_0^{z_*} dz \frac{1}{H(z)}. \tag{2.14}$$

Due to the interaction of DM with neutrino, the D_A or angular diameter distance varies, causing a shift in peak location with regard to the ΛCDM model. To determine the location of the peaks, we must reconcile the change in D_A. This is accomplished by altering the Hubble value. We may alter the Hubble value by expanding the parameter space for $N_{\rm eff}$ using equation (2.13). As a result of adding new relativistic components to the early Universe, the estimated value of H_0 increases [23, 50].

2.5 Conclusion

Cosmology plays an important role in measuring the nature of dark matter i.e., its particle properties. DM interaction with visible and dark sector produces a strong deviation from ΛCDM and imprints its signature on the angular and matter power spectrum.

Throughout the chapter, we reviewed the impact of DM-ν interaction on the CMB spectrum and matter power spectrum using a modified CLASS code. For this interaction we add an additional parameter u which shows the strength of this interaction along with the rest of the ΛCDM model parameters. DM interaction with neutrinos enhances angular power spectrum peaks and shifts their position towards higher multipole as this interaction alters DM clustering with respect to ΛCDM due to non-gravitational coupling with neutrinos. Its largest impact is visible on the matter power spectrum in terms of damping at large values of k. These results are model-independent and we can apply them to any theory (non-standard) which involves coupling between DM and neutrinos.

By adjusting the Hubble value along with DM-ν interaction, we check for the Hubble tension reduction upto 2σ value. This helps us to narrow down the gap between astrophysical and cosmological observations. Also, we observe that this adjusting with the Hubble value does not reconcile the Hubble tension in a precise way, this tension can be further reduced to some level by opening parameter space for N_{eff}.

Thus, present analysis can constrain the particle physics models that involve DM-ν interaction by constraining their parameters with the help of the latest cosmological dataset.

Appendices

Appendix A

Perturbation equations for massless neutrino

A.1 Necessary ingredients

Here, we will work in the Conformal Newtonian gauge. The generalized form of energy-momentum tensor in phase space is given as

$$T^{\mu\nu} = \int dP_1 dP_2 dP_3 (-g)^{-1/2} \frac{P_\mu P_\nu}{P^0} f(x^i, P_j, \tau), \tag{A.1}$$

$$\text{here} \qquad f(x^i, P_j, \tau) = f_0(q)[1 + (x^i, q, n_j, \tau)]. \tag{A.2}$$

In above equation $(A.1)$, P_j is conjugate momentum for x_i and $P_j = qn_j$. g is the determinant of $g_{\mu\nu}$ metric with $(-g)^{-1/2} = R^{-4}(1 - \psi + 3\phi)$. And $dP_1 dP_2 dP_3 = (1 - 3\phi) q^2 dq d\Omega$. So,

$$T^0_0 = -R^{-4} \int dq d\Omega \; q^2 \sqrt{q^2 + (mR)^2} f_0(q)(1 + \psi), \tag{A.3}$$

$$T^0_i = -R^{-4} \int dq d\Omega \; q^2 n_i f_0(q) \psi, \tag{A.4}$$

$$T^i_j = -R^{-4} \int dq d\Omega \; q^2 \frac{q^2 n_i n_j}{\sqrt{q^2 + (mR)^2}} f_0(q)(1 + \psi). \tag{A.5}$$

Above we have used $P_0 = R^2 \sqrt{(p^2 + m^2)}$ and $P_i = Rp_i$ here p_i is proper momentum and P_i is comoving momentum. ψ is perturbation potential source.

Now, from Boltzmann equation we have,

$$\frac{Df}{d\tau} = \frac{\partial f}{\partial \tau} + \frac{\partial f}{\partial x^i}\frac{dx^i}{d\tau} + \frac{\partial f}{\partial q}\frac{dq}{d\tau} + \frac{\partial f}{\partial n_i}\frac{dn_i}{dn_i} = \left(\frac{\partial f}{\partial \tau}\right)_C. \tag{A.6}$$

For simplicity we have dropped out the term, (x^i, q, n_j, τ). $\frac{\partial f}{\partial n_i}\frac{dn_i}{dn_i}$ is of second order, so we ignore it as we proceed only with linear perturbation terms.

Now, geodesics equation is given as

$$P^0 \frac{dP^\mu}{d\tau} + \Gamma_{\mu\alpha\beta} P^\alpha P^\beta = 0, \tag{A.7}$$

And Christoffel coefficients are given as,

$$\Gamma^\mu_{\nu\rho} = \frac{g^{\mu\nu}}{2}(\partial_\nu g_{\lambda\rho} + \partial_\rho g_{\lambda\nu} - \partial_\lambda g_{\nu\rho}) \tag{A.8}$$

with,

$$\Gamma^0_{00} = \mathcal{H} + \dot{\psi} \tag{A.9}$$

$$\Gamma^0_{0i} = \partial_i \psi \tag{A.10}$$

$$\Gamma^i_{00} = \delta^{ij} \partial_j \psi \tag{A.11}$$

$$\Gamma^0_{ij} = \mathcal{H}\delta_{ij} - [\dot{\phi} + 2\mathcal{H}(\phi + \psi)]\delta_{ij} \tag{A.12}$$

$$\Gamma^i_{j0} = \delta^i_j(\mathcal{H} - \dot{\phi}) \tag{A.13}$$

$$\Gamma^i_{jk} = -(\delta^i_j \partial_k + \delta^i_k \partial_j)\phi + \delta_{jk}\delta^{il}\partial_l \phi. \tag{A.14}$$

$$\tag{A.15}$$

Using geodesics equation and Christoffel coefficients we get

$$\frac{dq}{d\tau} = q\dot{\phi} - \epsilon n_i \partial_i \psi, \tag{A.16}$$

which can be written in momentum space as,

$$\frac{\partial \psi}{\partial \tau} + \iota \frac{q}{\epsilon}(\vec{k} \cdot \hat{n})\psi + \frac{d \ln f_0}{d \ln q}) \left[\dot{\phi} - \iota \frac{\epsilon}{q}(\vec{k} \cdot \hat{n})\psi\right] = \frac{1}{f_0}\left(\frac{\partial f}{\partial \tau}\right)_C. \tag{A.17}$$

Here, we have used $\partial_i = \iota(\vec{k} \cdot \hat{n})$ and $dx/x = d \ln x$.

A.2 Derivation of perturbation equations for ν

Now we will use above equations to find perturbation equations for mass-less neutrinos. Relation between energy density and pressure for ν is given for unperturbed case as

$$\bar{\rho} = 3\bar{P} = T^0_0 = T^i_i = R^{-4} \int dq d\Omega \; q^3 f_0(q). \tag{A.18}$$

So, density perturbation for ν is given as

$$\delta\rho_\nu = 3\delta P_\nu = R^{-4} \int dq d\Omega \; q^3 f_0(q)\psi, \tag{A.19}$$

Similarly velocity and shear stress perturbations can be given as

$$\delta T^0_{\nu i} = R^{-4} \int dq d\Omega \; q^3 n_i f_0(q)\psi, \tag{A.20}$$

$$\Sigma^i_{\nu j} = R^{-4} \int dq d\Omega \; q^3 \left(n_i n_j - \frac{1}{3}\delta_{ij}\right) f_0(q)\psi. \tag{A.21}$$

As $m_\nu = 0$, so $P_0 = \epsilon = q$. Integrating over q and expanding the angular dependence in terms of Legendre polynomial, the distribution function for neutrinos is given as

$$F_\nu(\vec{k}, \hat{n}, \tau) = \frac{\int dq q^3 f_0(q)\psi}{\int dq q^3 f_0(q)} = \sum_{l=0}^{\infty}(-\iota)^l (2l+1) F_{\nu l}(\vec{k}, \tau) P_l(\hat{k}\cdot\hat{n}). \tag{A.22}$$

Since $\delta_\nu = \delta\rho/\bar{\rho}$. So using eq. $(A.18)$ and eq. $(A.19)$ we get,

$$\delta_\nu = \delta\rho/\bar{\rho} = \frac{R^{-4}\int dq d\Omega\ q^3 f_0(q)\psi}{R^{-4}\int dq d\Omega\ q^3 f_0(q)} = \frac{1}{4\pi}\int d\Omega F_\nu = F_{\nu 0} \tag{A.23}$$

Similary $\theta_\nu = \frac{\delta T_i^0}{T_i^0}$ and $\sigma = \frac{2\bar{\rho}}{3(\bar{\rho}+\bar{P})}\Sigma$, gives

$$\theta_\nu = \frac{3\iota}{16\pi}\int d\Omega(\vec{k}\cdot\hat{n})F_\nu = \frac{3}{4}kF_{\nu l} \tag{A.24}$$

$$\sigma_\nu = \frac{-3}{16\pi}\int d\Omega\left[(\vec{k}\cdot\hat{n})^2 - \frac{1}{3}\right]F_\nu = \frac{1}{2}F_{\nu 2}. \tag{A.25}$$

Now, integrating equation $(A.17)$ over $dq\ q^3 f_0(q)$ and putting $1/f_0(\partial f/\partial\tau)_C = 0$ and then diving the obtained eq. with $\int dq\ q^3 f_0(q)$, we get

$$\frac{\partial F_\nu}{\partial \tau} + \iota k\mu F_\nu = 4(\dot{\phi} - \iota k\mu\psi). \tag{A.26}$$

Here. $\mu = \hat{k}\cdot\hat{n}$. From equation $(A.22)$ we get

$$F_{\nu l}(\vec{k}, \tau) = \iota^l \int_{-1}^{1}\frac{d\mu}{2}P_l(\mu)F_\nu(\vec{k}, \hat{n}, \tau). \tag{A.27}$$

Now, multiplying by $\int_{-1}^{1} d\mu P_l(\mu)$ in equation. $(A.26)$, and using recursion formula of Legendre polynomial along with equation $(A.27)$ we get

$$\dot{F_{\nu l}} - \frac{k}{2l+1}[lF_{\nu(l-1)} - (l+1)F_{\nu(l+1)}] = 2\iota^l\int_{-1}^{1} d\mu P_l(\mu)(\dot{\phi} - \iota k\mu\psi). \tag{A.28}$$

Putting values for $l = 1, 2, 3...$ separately we get,

$$\dot{\delta}_\nu = -\frac{4}{3}\theta_\nu + 4\dot{\phi}, \tag{A.29}$$

$$\dot{\theta}_\nu = k^2\left(\frac{1}{4}\delta_\nu - \sigma_\nu\right)\theta_{\rm DM} + k^2\psi - \left(\frac{4\rho}{3\rho_{\rm DM}}\right)\dot{\mu}(\theta_{\rm DM} - \theta_\nu), \tag{A.30}$$

$$\dot{F}_{\nu 2} = 2\dot{\sigma}_\nu = \frac{8}{15}\theta_\nu - \frac{3}{5}kF_{\nu 3} - \frac{9}{5}\dot{\mu}\sigma_\nu, \tag{A.31}$$

$$\dot{F}_{\nu l} = \frac{k}{(2l+1)}[lF_{\nu\ l-1} - (l+1)F_{\nu\ l+1}] - \dot{\mu}F_{\nu l}, \qquad l \geq 3. \tag{A.32}$$

Equation $(A.32)$ is followed for higher values of l.

Bibliography

[1] Hinshaw, Gary, et al. "Nine-year Wilkinson Microwave Anisotropy Probe (WMAP) observations: cosmological parameter results." The Astrophysical Journal Supplement Series 208.2 (2013): 19.

[2] Zwicky, Fritz. "Die rotverschiebung von extragalaktischen nebeln." Helvetica physica acta 6 (1933): 110-127.

[3] Aghanim, Nabila, et al. "Planck 2018 results-I. Overview and the cosmological legacy of Planck." Astronomy and Astrophysics 641 (2020): A1

[4] Jee, M. James, et al. "Hubble Space Telescope/Advanced Camera for Surveys confirmation of the dark substructure in A520." The Astrophysical Journal 783.2 (2014): 78.

[5] Grupen, C., Cowan, G., Eidelman, S. and Stroh, T., 2005. Astroparticle physics (Vol. 50). Berlin: Springer.

[6] Blagojević, Milutin, and Friedrich W. Hehl. "Gauge theories of gravitation." arXiv preprint arXiv:1210.3775 (2012).

[7] Arnau Romeu, Joan. "Derivation of Friedman equations." (2014).

[8] Kolb, Edward W., and Michael S. Turner. The early universe. CRC press, 2018.

[9] Anninos, Peter. "Computational cosmology: From the early universe to the large scale structure." Living reviews in relativity 4.1 (2001).

[10] Dolgov, A. D. "Big bang nucleosynthesis." Nuclear Physics B-Proceedings Supplements 110 (2002): 137-143.

[11] Bethke, Siegfried. "World Summary of αs (2012)." Nuclear Physics B-Proceedings Supplements 234 (2013): 229-234.

[12] Ichimasa, R., et al. "Big-Bang Nucleosynthesis in comparison with observed helium and deuterium abundances: possibility of a nonstandard model." Physical Review D 90.2 (2014): 023527.

[13] Fields, Brian D. "The primordial lithium problem." Annual Review of Nuclear and Particle Science 61 (2011): 47-68.

[14] Bobin, J., et al. "Joint Planck and WMAP CMB map reconstruction." Astronomy Astrophysics 563 (2014): A105.

[15] Penzias, Arno A., and Robert Woodrow Wilson. "A measurement of excess antenna temperature at 4080 Megacycle per second (Mc/s)." The Astrophysical Journal 142 (1965): 419-421.

[16] Pettini, M. "Introduction to cosmology: Basic concepts." Lecture notes, accessed online (2018). https://people.ast.cam.ac.uk/ pettini/Intro 20Cosmology/

[17] Mather, John C., et al. "Measurement of the cosmic microwave background spectrum by the COBE FIRAS instrument." The Astrophysical Journal 420 (1994): 439-444.

[18] Hinshaw, Gary, et al. "Nine-year Wilkinson Microwave Anisotropy Probe (WMAP) observations: cosmological parameter results." The Astrophysical Journal Supplement Series 208.2 (2013): 19.

[19] Kogut, Alan, et al. "Dipole anisotropy in the COBE DMR first-year sky maps." arXiv preprint astro-ph/9312056 (1993).

[20] Giunti, C. and Kim, C.W., 2007. Fundamentals of neutrino physics and astrophysics. Oxford university press.

[21] Seljak, U., and M. Zaldarriaga. "CMBFAST: A microwave anisotropy code." Astrophysics Source Code Library (1999): ascl-990

[22] Lewis, Antony, and Anthony Challinor. "Camb: Code for anisotropies in the microwave background." Astrophysics source code library (2011): ascl-1102.

[23] Lesgourgues, Julien. "The cosmic linear anisotropy solving system (CLASS) I: overview." arXiv preprint arXiv:1104.2932 (2011).

[24] Ryden, B., 2017. Introduction to cosmology. Cambridge University Press.

[25] Hu, W. and White, M., 1996. "Acoustic signatures in the cosmic microwave background." The Astrophysical Journal, 471(1), p.30.

[26] Keisler, R., et al. "A measurement of the damping tail of the cosmic microwave background power spectrum with the South Pole Telescope." The Astrophysical Journal 743.1 (2011): 28.

[27] McMaster, William H. "Polarization and the Stokes parameters." American Journal of Physics 22.6 (1954): 351-362.

[28] Baumann, Daniel, et al. "Probing inflation with CMB polarization." AIP Conference Proceedings. Vol. 1141. No. 1. American Institute of Physics, 2009.

[29] Hu, Wayne, Matthew M. Hedman, and Matias Zaldarriaga. "Benchmark parameters for CMB polarization experiments." Physical Review D 67.4 (2003): 043004.

[30] Frenk, Carlos S., and Simon DM White. "Dark matter and cosmic structure." Annalen der Physik 524.9-10 (2012): 507-534.

[31] Dodelson, Scott. Modern cosmology. Elsevier, 2003.

[32] Sofue, Yoshiaki. "Rotation curve of the Milky Way and the dark matter density." Galaxies 8.2 (2020): 37.

[33] Murayama, Hitoshi. "Physics beyond the standard model and dark matter." arXiv preprint arXiv:0704.2276 (2007).

[34] Metcalf, R. Benton, and Piero Madau. "Compound gravitational lensing as a probe of dark matter substructure within galaxy halos." The Astrophysical Journal 563.1 (2001): 9.

[35] Clowe, Douglas, Anthony Gonzalez, and Maxim Markevitch. "Weak-lensing mass reconstruction of the interacting cluster 1e 0657–558: Direct evidence for the existence of dark matter." The Astrophysical Journal 604.2 (2004): 596.

[36] Brownstein, J. R., and J. W. Moffat. "The Bullet Cluster 1E0657-558 evidence shows modified gravity in the absence of dark matter." Monthly Notices of the Royal Astronomical Society 382.1 (2007): 29-47.

[37] Alcock, Charles, et al. "MACHO Project Limits on Black Hole Dark Matter in the 1-30 M Range." The Astrophysical Journal 550.2 (2001): L169.

[38] Buchmüller, Oliver, Matthew J. Dolan, and Christopher McCabe. "Beyond effective field theory for dark matter searches at the LHC." Journal of High Energy Physics 2014.1 (2014): 1-24.

[39] Gaitskell, Richard J. "Direct detection of dark matter." Annu. Rev. Nucl. Part. Sci. 54 (2004): 315-359.

[40] Aprile, Elena, et al. "Xenon." Nuclear Physics B-Proceedings Supplements 173 (2007): 113-116.

[41] Atwood, W. B., et al. "The large area telescope on the Fermi gamma-ray space telescope mission." The Astrophysical Journal 697.2 (2009): 1071.

[42] Dawson, Kyle S., et al. "The Baryon oscillation spectroscopic survey of SDSS-III." The Astronomical Journal 145.1 (2012): 10.

[43] Norberg, Peder, et al. “The 2dF Galaxy Redshift Survey: luminosity dependence of galaxy clustering.” Monthly Notices of the Royal Astronomical Society 328.1 (2001): 64-70.

[44] Blake, Chris, et al. “The WiggleZ Dark Energy Survey: mapping the distance–redshift relation with baryon acoustic oscillations.” Monthly Notices of the Royal Astronomical Society 418.3 (2011): 1707-1724.

[45] Ma, Chung-Pei, and Edmund Bertschinger. “Cosmological perturbation theory in the synchronous and conformal Newtonian gauges.” arXiv preprint astro-ph/9506072 (1995).

[46] Wilkinson, Ryan J., Celine Boehm, and Julien Lesgourgues. “Constraining dark matter-neutrino interactions using the CMB and large-scale structure.” Journal of Cosmology and Astroparticle Physics 2014.05 (2014): 011.

[47] Paul, Arnab, et al. “Shedding light on dark matter and neutrino interactions from cosmology.” Journal of Cosmology and Astroparticle Physics 2021.10 (2021): 017.

[48] Ghosh, Subhajit, Rishi Khatri, and Tuhin S. Roy. “Dark neutrino interactions make gravitational waves blue.” Physical Review D 97.6 (2018): 063529.

[49] Cyr-Racine, Francis-Yan, et al. “Constraints on large-scale dark acoustic oscillations from cosmology.” Physical Review D 89.6 (2014): 063517.

[50] Ghosh, Subhajit, Rishi Khatri, and Tuhin S. Roy. “Can dark neutrino interactions phase out the Hubble tension?” Physical Review D 102.12 (2020): 123544.

[51] Serra, Paolo, et al. “Constraints on neutrino-dark matter interactions from cosmic microwave background and large scale structure data.” Physical Review D 81.4 (2010): 043507.

[52] Stadler, Julia, Céline Bœhm, and Olga Mena. “Comprehensive study of neutrino-dark matter mixed damping.” Journal of Cosmology and Astroparticle Physics 2019.08 (2019): 014.

[53] Viel, Matteo, et al. “Warm dark matter as a solution to the small scale crisis: New constraints from high redshift Lyman- forest data.” Physical Review D 88.4 (2013): 043502.

[54] Vogt, Steven S., and G. Donald Penrod. “HiRES: A high resolution Echelle spectrometer for the Keck 10-meter telescope.” Instrumentation for Ground-Based Optical Astronomy. Springer, New York, NY, 1988. 68-103.

[55] Bernstein, Gary M., et al. “Volume-phase holographic spectrograph for the Magellan telescopes.” Optical Spectroscopic Techniques, Remote Sensing, and Instrumentation for Atmospheric and Space Research IV. Vol. 4485. SPIE, 2002.

[56] Vagnozzi, Sunny. “New physics in light of the H_0 tension: an alternative view.” Physical Review D 102.2 (2020): 023518.

[57] Di Valentino, Eleonora, et al. “In the Realm of the Hubble tension − a Review of Solutions.” arXiv preprint arXiv:2103.01183 (2021).

[58] Verde, Licia, Tommaso Treu, and Adam G. Riess. “Tensions between the early and late Universe.” Nature Astronomy (2019): 891-895.

[59] Scoville, Nick, et al. “COSMOS: Hubble space telescope observations.” The Astrophysical Journal Supplement Series 172.1 (2007): 38.

[60] Collaboration, Planck, et al. “Planck 2018 results. VI. Cosmological parameters.” (2020).